Comparative anatomy of the carotid canal in the Miocene small-bodied catarrhine *Pliobates cataloniae*

Abstract

The small-bodied Miocene catarrhine *Pliobates cataloniae* (11.6 Ma, Spain) displays a mosaic of catarrhine symplesiomorphies and hominoid synapomorphies that hinders deciphering its phylogenetic relationships. Based on cladistic analyses it has been interpreted as a stem hominoid or as a pliopithecoid. Intriguingly, the carotid canal orientation of *Pliobates* was originally described as hylobatid-like. The variation in carotid canal morphology among anthropoid clades shown in previous studies suggests that this structure might be phylogenetically informative. However, its potential for phylogenetic reconstruction among extinct catarrhines remains largely unexplored. Here we quantify the orientation, proportions, and course of the carotid canal in *Pliobates*, extant anthropoids and other Miocene catarrhines (*Epipliopithecus*, *Victoriapithecus,* and *Ekembo*) using 3D morphometric techniques. We also compute phylogenetic signal and reconstruct the ancestral carotid canal course for main anthropoid clades. Our results reveal that carotid canal morphology embeds strong phylogenetic signal but mostly discriminates between platyrrhines and catarrhines, with an extensive overlap among extant catarrhine families. The analyzed extinct taxa display a quite similar carotid canal morphology more closely resembling that of extant catarrhines. Nevertheless, our results for *Pliobates* highlight some differences compared with the pliopithecid *Epipliopithecus*, which displays a somewhat more platyrrhine-like morphology. In contrast, *Pliobates* appears as derived toward the modern catarrhine condition as the stem cercopithecid *Victoriapithecus* and the stem hominoid *Ekembo*, which more closely resemble one another. Moreover, *Pliobates* appears

somewhat derived toward the reconstructed ancestral hominoid morphotype, being more similar than other Miocene catarrhines to the condition of great apes and the hylobatid *Symphalangus*. Overall, our results rule out previously noted similarities in carotid canal morphology between *Pliobates* and hylobatids, but do not show particular similarities with pliopithecoids either—as opposed to extant and other extinct catarrhines. Additional analyses will be required to clarify the phylogenetic relationships of *Pliobates*, particularly given its dental similarities with dendropithecids.

Keywords: Internal carotid artery; Petrosal; Geometric morphometrics; Fossil primates; Phylogeny; Evolution.

1. Introduction

1.1. Pliobates *and catarrhine evolution*

Crown catarrhines include two main extant clades distinguished at the superfamily rank: Old World monkeys (Cercopithecoidea) and apes and humans (Hominoidea). Earliest stem catarrhines have been reported from the latest Eocene (34.5–29.5 Ma) of Afro-Arabia (Seiffert, 2006, 2012; Seiffert et al., 2010). In turn, earliest crown catarrhines (both cercopithecoids and hominoids) date back to the late Oligocene (~25 Ma) of East Africa (Stevens et al., 2013)—in accordance with molecular estimates indicating that the cercopithecoid–hominoid divergence occurred during the Oligocene (Chatterjee et al., 2009; Perelman et al., 2011; Springer et al., 2012; Finstermeier et al., 2013; Pozzi et al., 2014). Catarrhines did not disperse into Eurasia until later in the early Miocene, following the closure of the Tethys Seaway and the establishment of intermittent land bridges at ~19 Ma (Harzhauser et al., 2007; Harrison, 2013). Several catarrhine lineages eventually dispersed

from Afro-Arabia into Eurasia (Roos et al., 2019; Gilbert et al., 2020a), including: pliopithecoids (considered an Eurasian clade of stem catarrhines, first recorded ~18–17 Ma; Harrison and Gu, 1999; Begun, 2002, 2017; Harrison, 2013); hylobatids (first recorded ~13.8–12.5 Ma; Gilbert et al., 2020b); large-bodied hominoids (presumably hominids, first recorded ~16.5–14 Ma; Casanovas-Vilar et al., 2011; Harrison, 2017); and various lineages of cercopithecoid primates, successively recorded at different times in Eurasia, namely colobines (~8.5 Ma; Alba et al., 2015a), cercopithecins (~8–6.5 Ma; Gilbert et al., 2014), macaques (~5.9–5.3 Ma; Alba et al., 2014a), and geladas (1.6–1.2 Ma; Alba et al., 2014b).

A panoply of small-bodied, putative stem catarrhine genera (including, but not restricted to, dendropithecids) are recorded in the early to middle Miocene of Africa (Harrison, 2010, 2013). Some Miocene Eurasian taxa have previously been linked to some of these African stem catarrhines—implying yet another catarrhine dispersal event from Africa—but such claims have been mostly rejected by reinterpreting them as pliopithecoids or hylobatids (Harrison, 2016 and references therein). The most likely exception is some isolated dental remains from Pakistan (~17–16 Ma; Barry et al., 1987; Bernor et al., 1988), which are most similar to African dendropithecids (Harrison, 2016) but might ultimately prove to be stem pliopithecoids (Sankhyan et al., 2017). In turn, as remarked by Roos et al. (2019), the small-bodied catarrhine *Pliobates* (middle/late Miocene of Spain, 11.6 Ma; Alba et al., 2015b) might denote an additional out-of-Africa dispersal event of catarrhines unless it is interpreted as a pliopithecoid. This taxon was originally recovered by Alba et al.'s (2015b) cladistic analysis as a stem hominoid morphologically more derived than *Proconsul* s.l. (currently split into *Proconsul* s.s. and *Ekembo*; McNulty et al., 2015) and subsequently reinterpreted as a pliopithecoid by different cladistic analyses (Nengo et al., 2017; Gilbert et al., 2020b), as first suggested by Benefit and McCrossin (2015). However, given the mosaic

nature of its cranial and postcranial skeleton—combining plesiomorphic, stem catarrhine-like features (including dental resemblances with dendropithecids) with crown hominoid synapomorphies (Alba et al., 2015b)—the possibility remains that *Pliobates* is a late descendant of an African stem catarrhine lineage.

Deciphering the phylogenetic position of *Pliobates* would have important implications for our current understanding of catarrhine evolution and paleobiogeography during the Miocene. If ultimately shown to be a pliopithecoid or as a member of a different stem catarrhine lineage, it would imply remarkable cranial and postcranial convergences with crown hominoids; in turn, if interpreted as a non-pliopithecoid stem catarrhine or as a stem hominoid, it would indicate that pliopithecoids were not the only small catarrhines to disperse from Africa into Europe. Unfortunately, determining the evolutionary history and phylogenetic relationships of small-bodied catarrhines is still hindered by the fragmentary nature of their fossil remains and the incompleteness of their fossil record—with long ghost lineages for both pliopithecoids and hylobatids. Deciphering the phylogenetic position of extinct taxa ultimately requires performing cladistic analyses with all available evidence from multiple anatomical regions. However, as mentioned above, previous attempts in this regard have yielded contradictory results for *Pliobates* (compare Alba et al., 2015b with Nengo et al., 2017 and Gilbert et al., 2020b). Therefore, additional research on the various characters included in these analyses is required to refine their definition and scoring for both extant and extinct taxa. With this aim in mind, here we focus on one of the most intriguing features included in the original diagnosis of *Pliobates*: the orientation of the carotid canal, which was originally described as most closely resembling hylobatids than either pliopithecoids or other hominoids (Alba et al., 2015b). Given the potential implications of such similarities—if interpreted as a hylobatid synapomorphy or hominoid symplesiomorphy—we decided to

analyze them quantitatively by means of a novel morphometric approach devised to measure the size and shape of the carotid canal. To the best of our knowledge, this is the first study to quantitatively assess the orientation, proportions, and course of this anatomical structure in extant and extinct anthropoids.

1.2. The carotid canal in primate phylogenetics

All haplorrhines and non-cheirogaleid lemuriforms have an internal carotid artery enclosed by a bony canal (termed 'carotid canal') that derives from the anterior lamina of the petrosal plate (Bugge, 1974, 1980; Cartmill et al., 1981; MacPhee and Cartmill, 1986; Kay et al., 2008; Boyer et al., 2016). The carotid canal runs from the posterolaterally located external carotid foramen to the endocranial space (Bugge, 1980; MacPhee and Cartmill, 1986; Kay et al., 2008; Boyer et al., 2016). In haplorrhines, the carotid canal displays a 'perbullar pathway': it is located in the primary medial wall of the auditory bulla and runs through the middle ear cavity, passing through the transverse septum that separates the tympanic cavity from the anterior accessory cavity (Cartmill et al., 1981; MacPhee and Cartmill 1986; Kay et al., 2008). The canal then opens more anteromedially into the endocranial surface, with an opening located either on the basisphenoid or between the basisphenoid and petrosal (Boyer et al., 2016). In adult anthropoids, one of the two branches of the internal carotid artery (the stapedial artery) is missing and only the promontory artery remains patent (Bugge 1974, 1980; Rosenberger and Szalay, 1980; MacPhee and Cartmill, 1986; Kay et al., 2008; Boyer et al., 2016). Therefore, the carotid canal of anthropoid primates corresponds to a unique and well-developed bony enclosure.

Low homoplasy is one of the most important criteria for choosing phylogenetically informative morphological characters (Lieberman, 1999). Among characters least affected by

121 homoplasy (convergence, parallelism, reversal, and homoiology), soft-tissue traits have
122 previously been proven more efficient in producing accurate primate phylogenies than hard-
123 tissue traits (Gibbs et al., 2000, 2002; Diogo and Wood, 2011). Given that vessel and nerve-
124 related characters are soft-tissue traits, this rationale might potentially apply to the carotid
125 canal as well. A few previous studies have included carotid canal features in character-taxon
126 matrices devised for cladistic analysis, focusing on the position of the carotid foramen in the
127 bulla as well as on the overall direction and orientation of the canal itself (Beard and
128 MacPhee, 1994; Ross, 1994; Shoshani et al., 1996; Ross et al., 1998; Kay et al., 2008; Alba et
129 al., 2015b). These studies aimed at resolving phylogenetic relationships among higher-rank
130 primate clades (Beard and MacPhee, 1994; Ross, 1994; Shoshani et al., 1996; Ross et al.,
131 1998; Kay et al., 2008) and/or deciphering the phylogenetic relationships of particular fossil
132 taxa (Ross et al., 1998; Kay et al., 2008; Alba et al., 2015b). Nonetheless, some of them found
133 differences between platyrrhines and catarrhines, as well as among some catarrhine groups.
134 Based on these studies, the morphology of the carotid canal seems promising for
135 phylogenetic reconstruction in catarrhine primates. However, the exact phylogenetic
136 potential of this structure for distinguishing among catarrhine subclades and, hence,
137 clarifying the relationships of extinct taxa remains unexplored.

138 In the light of all the considerations above, the aim of this paper is threefold: (1)
139 investigate the orientation, proportions, and course of the carotid canal in a wide sample of
140 extant anthropoid primates, to test its potential for phylogenetic inference in extinct
141 catarrhines; (2) re-evaluate previously noted differences and similarities among several
142 catarrhine clades; and (3) describe the carotid canal morphology of *Pliobates* and compare it
143 with that of extant and fossil catarrhines, so as to gain additional insight on the controversial
144 phylogenetic relationships of this genus. To do so, we collected µCT scans of both fossil taxa

and an extant comparative sample, and developed a newly devised semiautomatic iterative protocol to obtain comparable 3D carotid canal surfaces (i.e., 3D models). These are analyzed by means of traditional morphometrics and three-dimensional geometric morphometric (3DGM) and imaging techniques, to quantify the orientation, proportions, and course of the carotid canal within the petrosal in a standardized manner.

2. Materials and methods

2.1. Materials

Studied sample This study focuses on the cranium of the holotype (IPS58443) of *Pliobates cataloniae*, which consists of a partial skeleton (Alba et al., 2015b). The carotid canal is entirely preserved in the right temporal fragment (IPS58443.1; Alba et al., 2015b: Fig. 1A). In contrast, in the left temporal fragment (same specimen) the inferiormost part of the canal is broken, with most of its lateral and anterior walls missing along a length of >1.5 mm. IPS58443.1 was originally scanned at a resolution of 95 µm (Alba et al., 2015b). To explore fine bony structures, the specimen was scanned again by X-ray microtomography at the Centro Nacional de Investigación sobre la Evolución Humana (CENIEH, Burgos, Spain) using a Phoenix V|Tome|X s240 µCT scanner with the following parameters: 0.35 mA current, 170 kV voltage, 0.2 mm Cu filter, and a magnification of 9.52. The final reconstructed volume has an isometric voxel size of 21 µm.

Fossil comparative sample Three Miocene catarrhines are included in the comparative sample: the Miocene pliopithecoid *Epipliopithecus vindobonensis* (see Zapfe, 1961), the stem cercopithecoid (victoriapithecid) *Victoriapithecus macinnesi* (see review in Benefit and McCrossin, 1997), and the stem hominoid (proconsulid) *Ekembo heseloni* (see review in McNulty et al., 2015). There are four available fragmentary temporal bones of

Epipliopithecus (Zapfe, 1961): NMB OE 303 (right and left temporals, individual II), NHMW 1970/1397/0002 (right temporal, individual III; holotype), and NHMW 1970/1397/0003 (left temporal, individual III; holotype). The carotid canal is only sufficiently preserved in the latter specimen, which includes a portion of the bulla, the external acoustic meatus, and most of the petrosal (Zapfe, 1961: Fig. 28). In contrast, the anterior end of the canal is missing from the remaining specimens. The petrosal of the holotype was scanned at the Vienna µCT lab (Vµ-CTL) using a Viscom X8060 µCT scanner with the following parameters: 0.24 mA current, 120 kV voltage, 0.5 mm Cu filter, and a magnification of 7.50. The final reconstructed volume has an isometric voxel size of 22 µm. *Ekembo heseloni* is represented by the right temporal specimen KNM-RU 2036al (Davis and Napier, 1963: Fig. 1; Alba et al., 2015b: Fig. 4C), which is part of the holotype (Walker et al., 1993), while *V. macinnesi* is represented by the left temporal of the cranium KNM-MB 29100 (Benefit and McCrossin, 1997: Fig. 1; Benefit, 1999: Fig. 3; Jablonski and Frost, 2010: Fig. 23.1). The µCT scans of KNM-RU 2036al and KNM-MB 29100 have isometric voxel sizes of 64 µm and 44 µm, respectively. They were both kindly made available for this study by the Department of Earth Sciences, National Museums of Kenya (which holds the copyright) and the Department of Human Evolution, Max Plank Institute for Evolutionary Anthropology, Leipzig, Germany.

Extant comparative sample Our extant comparative sample consists of µCT scans of 127 crania belonging to 41 anthropoid species (13 platyrrhines and 28 catarrhines) from 36 genera, representing all extant hominoid genera as well as all cercopithecoid subtribes and platyrrhine (sub)families (Table 1; Supplementary Online Material [SOM] Table S1). A minimum of three individuals per genus are included. Ontogenetic changes in basicranial angulation and elongation—somewhat related to each other and potentially affecting petrosal morphology—continue up to adulthood as measured by M^3 eruption (Lieberman

and McCarthy, 1999; Lieberman et al., 2000). Therefore, all individuals included in the comparative sample are fully adult (exhibiting the M^3 in occlusion, or the M^2 in callitrichines). Most of the µCT scans included in our extant comparative sample were downloaded from MorphoSource (https://www.morphosource.org; Table 1; SOM Table S1). Three µCT scans of specimens from the AMNH were kindly provided by Sergio Almécija, while seven additional µCT scans of specimens housed in the Institut Català de Paleontologia Miquel Crusafont (Sabadell, Spain) were scanned at the CENIEH. The µCT resolution for the specimens included in the extant comparative sample ranges from 27 to 131 µm (Table 1; SOM Table S1).

2.2. Morphometric methods

Segmentation For each specimen, the carotid canal was virtually extracted through semiautomatic threshold-based segmentation in Avizo v. 7.0 (Visualization Sciences Group, Mérignac). The right carotid canal was segmented for most specimens; when this was not possible, the left canal was segmented and mirrored. Both extremities of the resulting 3D canal surfaces (i.e., 3D models) were cut along homologous planes to allow their comparison among different individuals. First, to cut the posterior end of the canal, we used a best-fit plane based on landmarks placed on its external aperture (Fig. 1a, l; SOM Fig. S1a, b). Then, the anterior limit of the carotid canal was identified by determining a landmark on the anterior part of the petrosal (the 'intersection ridge–groove' [IRG]; Fig. 1b–l; SOM Fig. S1c, d; see SOM S1) and cut through such a homologous point using a script coded in R v. 4.0.2 (R Core Team, 2020; see SOM file S1).

Alignment and canal orientation The orientation of the carotid canal within the petrosal was quantified by means of two 2D angles representing the canal superior orientation along the

(para)sagittal plane (2DYZA) and its medial orientation along a transverse plane (2DXYA)—which can be related to canal 'orientation' and 'direction' sensu Alba et al. (2015b: Tables S5 and S6), respectively. Each was computed as the angle between the vector connecting the canal endpoints (from posterior to anterior) and a standard reference vector. Both the canal vector and the reference vector were computed after performing a Procrustes alignment based on petrosal/tympanic landmarks (Fig. 2; Table 2) and applying the translation-scaling-rotation parameters resulting from this alignment to the two canal endpoints (SOM S1). This procedure allowed us to retain the information on the position, orientation and shape variation of the canal inside the petrosal. For both angles, the standard reference vector corresponds to a 2D vector parallel to the anteroposterior cranial axis (from posterior to anterior), in lateral view for 2DYZA and in superior view for 2DXYA (Fig. 3). Aligning the carotid canal on the basis of petrosal/tympanic landmarks instead of the cranium as a whole enables the analysis of fragmentary fossils and has several advantages (see SOM S1 for further details), while being consistent with previous studies (Beard and MacPhee, 1994; Ross, 1994; Shoshani et al., 1996; Ross et al., 1998; Kay et al., 2008; Alba et al., 2015b) that assessed carotid foramen locations relative to the bulla instead of general cranial axes or planes.

Volume and length The volume (V, in mm^3) of the 3D canal surfaces was computed using the module 'Surface Area Volume' in Avizo. To calculate canal length (L, in mm), we used equidistant slices between the two canal endpoints (which correspond to type III landmarks; Bookstein, 1991). These slices were used to generate 8 additional equidistant semilandmarks that follow the canal streamline using the 'digit.curve' function of 'Geomorph' v. 3.3.1 (Adams et al., 2019), summing a total of 10 canal landmarks, which define the canal streamline. This canal landmark configuration thus corresponds to a total of 10 canal

streampoints. Canal length was taken as the sum of the length of the resulting nine canal segments (see SOM S1 for further details).

Robusticity index Carotid canal proportions were measured by a dimensionless index of canal robusticity as $L/V^{1/3}$. Even though the carotid canal is a hollow structure, we refer to this index as 'robusticity' because it measures how thick the canal is on average relative to its length. Low values of the index denote robust canals, whereas high values denote slender canals. The same terms have been applied to other hollow cranial structures, such as the semicircular canals of the bony labyrinth (Urciuoli et al., 2020, 2021a, 2021b). The diameter (and hence the cross-sectional area) of the carotid canal varies along its length, so that using the cube root of the volume as the denominator is equivalent to relying on the hypothetical average cross-sectional area. We used the cube root of the volume to make the index dimensionless (i.e., a shape variable), and verified that the robusticity index was free from allometric (size-scaling) effects by computing a phylogenetic generalized least-squares (PGLS) regression of ln L against ln $V^{1/3}$ on the species means of the whole sample. We further computed a major axis regression of the same parameters, using the function 'lmodel2' of the R package 'lmodel2' v. 1.7-3 (Legendre, 2018). The objective was to test whether length and volume of the carotid canal covary in a linear (i.e., isometric) or non-linear (i.e., allometric) fashion, and to do so under the assumptions that the independent variable is measured with error (major axis) or without error (PGLS). Note that, under geometric similarity, linear dimensions and volumes are expected to be correlated with an allometric slope of 1/3 (Gould, 1966). However, this does not apply here because we used the cube root of the canal volume, so that allometry would imply an allometric slope significantly different from 1.

Canal course configuration To assess carotid canal course within the petrosal, we applied the translation-scaling-rotation parameters resulting from the alignment of the petrosal/tympanic landmarks described above to the 10 canal landmark configuration. As for canal orientation, we were able to retain the position, orientation and shape variation of the canal inside the petrosal. Therefore, the postalignment 10 canal landmark configuration represents the course of the carotid canal within the petrosal (SOM S1) and will be thereafter referred to as 'carotid canal course configuration'.

Size scaling To better understand the influence of size-scaling (allometric) effects on carotid canal shape, we computed multiple bivariate regressions using PGLS. On the one hand, we relied on allometric regressions of canal measurements (as measured by L and $V^{1/3}$) against overall canal size (as measured by centroid size [CS]; see Section 2.3 below) and body size (as measured by body mass [BM]); the allometric regression between CS and BM was also computed. On the other hand, we computed regressions between carotid canal shape—including not only the above-mentioned index of canal robusticity, but also the multivariate shape variables derived by means of between-group principal component analysis (bgPCA; see Section 2.3 below)—against log-transformed carotid canal size (as measured by $V^{1/3}$ and CS) and BM. To minimize the effects of body size dimorphism, for each taxon we relied exclusively on average female BM taken from the literature (Smith and Jungers, 1997; Delson et al., 2000; Turner et al., 2018). Natural logarithms (ln) were used in all instances. For allometric regressions between metrical linear variables, the null hypothesis of isometry was rejected when unity was excluded from the 95% CI of the allometric slope. In contrast, for bivariate regressions of shape vs. size, isometry was rejected when the regression was significant (i.e., when the slope was significantly different from zero).

288 *2.3. Between-group principal component analyses*

289 Carotid canal course variation among clades was examined using a bgPCA of the carotid
290 canal course configurations using the 'groupPCA' function of the R package 'Morpho' v. 2.8
291 (Schlager, 2017). We used the following four main crown anthropoid clades as grouping
292 factor: platyrrhines, cercopithecids, hylobatids, and hominids, with fossils projected onto the
293 morphospace a posteriori. The bgPCA analysis was repeated based on a catarrhine-only
294 subsample to see if it provided a better discrimination among extant catarrhine families
295 once the variance introduced by platyrrhines was removed.

296 As explained in the preceding section, allometric effects on canal course configuration
297 were assessed by means of PGLS regressions of between-group principal component (bgPCs)
298 against log-transformed canal size (ln CS and ln $V^{1/3}$) or log-transformed body size (ln BM)—
299 see Section 2.2 for further details.

300 We verified that the bgPCA grouping structure was not spurious by comparing our bgPCA
301 results with those of a cross-validated bgPCA (Cardini et al., 2019). This procedure iteratively
302 resamples the data set by excluding one individual at a time and using the remaining (n – 1)
303 individuals to compute the model that is then used to classify the omitted individual. A
304 cross-validated bgPCA significantly reduces the distortion of mean group differences, so that
305 its comparison with the non-cross-validated bgPCA allows one to ascertain whether (or to
306 what extent) the latter is affected by spurious grouping effects. As further recommended by
307 Cardini and Polly (2020), we also relied on a permutational analysis of variance
308 (PERMANOVA) to (1) explore the significance (p) of group mean differences and (2) compute
309 the variance (R^2) explained by them. The permutations consist in randomly resampling n
310 times the data set (thus modifying group composition, as the individuals are permuted),
311 each time recomputing the distance between the centroids of all pairs of newly formed

groups. Based on this set of permutations, here consisting of between-group Euclidean distances, both *p* and R^2 were computed within the full space of canal course configurations as well as within the bgPCA spaces (both standard and cross-validated bgPCs). As in the case of the cross-validated bgPCA scatterplot, comparing the *p* and R^2 values of the bgPCA (before and after cross-validation) with those of the raw canal course configuration coordinates permits verifying if the former inflates the differences among groups. These computations were done using the 'lm.rrpp' function of the R package 'RRPP' v. 0.6.1 (Collyer and Adams, 2018).

The discrimination among a priori defined groups was evaluated on the basis of correctly classified individuals after cross-validation. Posterior probabilities of group membership were computed for fossil specimens based on the squared Mahalanobis distances between their bgPC scores (bgPC1 and bgPC2) and those of extant group centroids using the 'typprobClass' function of 'Morpho'. Finally, a neighbor-joining (NJ) cluster was computed using a matrix of Euclidean distances based on the raw coordinates of the canal course configurations with the 'nj' function of the R package 'phangorn' v. 2.5.5 (Schliep, 2011).

2.4. Statistical analyses

Box and whisker plots were employed to assess the variation in carotid canal orientation (2DYZA and 2DXYA), proportions (index $L/V^{1/3}$), and course (bgPC1 and bgPC2). To test for significant differences among extant groups, we used Kruskal-Wallis non-parametric tests and Bonferroni-corrected Mann-Whitney post hoc pairwise comparisons performed in R. When significant differences were found, *Pliobates* and other extinct genera were compared with the distributions of extant groups using z-scores—computed as z = (individual value –

group mean) / SD—to assess if the fossil specimens fall within the variation of the latter ($|z| \leq 1.96$).

2.5. Phylogenetically informed methods

Phylogenetic tree To compute PGLS regressions and the phylomorphospaces, as well as to quantify phylogenetic signal, we used a time-calibrated phylogenetic tree among the investigated taxa. The tree for the extant taxa was primarily derived from the 10kTrees v.3 website (Arnold et al., 2010), although some species that were not included there were added a posteriori following Meyer et al. (2011) and Springer et al. (2012)—see SOM S1 for further details. Two different hypotheses for the extinct genera were considered, except for *Victoriapithecus*, which was invariably considered a stem cercopithecoid. Under hypothesis 1 (SOM Fig. S2a), *Epipliopithecus, Ekembo*, and *Pliobates* were considered successive stem hominoids, following the results of Alba et al.'s (2015b) cladistic analysis. In contrast, under hypothesis 2 (SOM Fig. S2b), only *Ekembo* was considered a stem hominoid, while both *Pliobates* and *Epipliopithecus* were considered stem catarrhines (pliopithecoids), following the results of other cladistic analyses (Nengo et al., 2017; Gilbert et al., 2020b). The tip and divergence dates for the extinct taxa are detailed in SOM S1.

Phylogenetic signal To assess the phylogenetic signal embedded in carotid canal course, we computed Pagel's λ (Pagel, 1999) and Blomberg's K (Blomberg et al., 2003) statistics using the R package 'phytools' v. 0.7-70 (Revell, 2012). These metrics compare the variance in the phylogenetic tree tips relative to that expected under a Brownian motion evolutionary model. Pagel's λ measures the covariance among related species and ranges from 0 (no phylogenetic signal) to 1 (high phylogenetic signal). In turn, Blomberg's K reflects to what extent the phylogenetic tree matches the variance in the data (and where variance is

concentrated): $K \approx 1$ means that trait evolution approximates the expectations under a Brownian motion model; $K \ll 1$ means that closely related taxa resemble each other less than expected under a Brownian motion model (such that variance is mostly found within clades); finally, $K \gg 1$ means that closely related units resemble each other more than expected under a Brownian motion model (such that variance is mostly found among clades).

Phylomorphospace and reconstruction of ancestral morphotypes To quantify and visualize patterns of carotid canal course variation along the branches of the phylogeny, we produced a phylomorphospace by projecting the phylogenetic tree onto the two first bgPCs (Sidlauskas, 2008). In a phylomorphospace, the taxon centroids are connected to one another in the morphospace following the phylogenetic relationships given by the chosen phylogeny. In the case of fossil taxa, because there are competitive hypotheses regarding their phylogenetic relationships, various time-calibrated cladograms were devised a priori—resulting in a different phylomorphospace for each phylogenetic hypothesis. Scores of the internal nodes—last common ancestors (LCAs)—were estimated based on a maximum likelihood method for continuous characters using the 'fastAnc' function of 'phytools'. To explore the extent to which extant and extinct taxa differ from the various LCAs, we rotated and translated the bgPC scores estimated for the LCAs back into the Kendall's shape space (i.e., configuration space) to obtain their landmarks coordinates and thus visualize the estimated ancestral carotid canal course conformations.

3. Results

The 3D carotid canal surface of *Pliobates* (SOM File S2) is compared with those of *Ekembo*, *Epipliopithecus*, and *Victoriapithecus*, as well as selected taxa from the extant

383 comparative sample in Figure 4. Individual data for the variables describing the orientation,
384 proportions, and course of the carotid canal in the extant comparative sample are reported
385 in SOM Table S2.
386
387 *3.1. Carotid canal orientation*
388 For 2DYZA, the angle values range from ca. 30° to 90° (Fig. 5a; Tables 3 and 4). On this
389 basis, and taking into account the mean extant clade differences (SOM Tables S3 and S4), we
390 defined three different states (potentially usable in future cladistic analyses): oblique (<55°);
391 subvertical (55–65°); and vertical (>65º). Hominoids have smaller angles than platyrrhines
392 and cercopithecids, i.e., a less vertically oriented canal, whereas cercopithecids have the
393 highest angles, corresponding to vertical canals (Fig. 5a; Table 3; SOM Tables S3 and S4).
394 *Pliobates* has the lowest value among Miocene catarrhines and does not significantly differ
395 from the hylobatid range of variation (Fig. 5a; Tables 4 and 5). *Epipliopithecus* and *Ekembo*
396 display very similar values to one another and most closely fit with the hominoid variation,
397 although they only significantly differ from cercopithecids (Fig.5a; Tables 4 and 5). In
398 contrast, *Victoriapithecus* has a higher angle, more similar to the monkey condition (i.e., a
399 more vertical canal; Fig.5a; Table 4), although it does not significantly differ from any extant
400 group (Table 5).
401 In the case of 2DXYA, the values range from ca. -4° to 45° (Fig. 5a; Tables 3 and 4; see
402 SOM S1 regarding the interpretation of negative angles). On this basis, and taking into
403 account the mean differences among extant clades (SOM Tables S3 and S4), we defined two
404 discrete states: anteriorly oriented (≤30°); and medially oriented (>30°). Despite some
405 overlap, platyrrhines display a significantly higher 2DXYA—i.e., a more medially (less
406 anteriorly) directed canal—than the three catarrhine families, which do not differ

significantly from one another (Fig. 5b; Table 3; SOM Tables S3 and S4). Among the fossil specimens, *Ekembo* shows the highest 2DXYA whereas *Victoriapithecus* shows the lowest (Fig.5b; Table 4). Based on the z-scores (Table 5), *Ekembo* displays a higher angle than extant hominoids, *Victoriapithecus* and *Pliobates* show a lower angle than extant platyrrhines, and *Epipliopithecus* displays a higher angle than hylobatids.

3.2. Carotid canal proportions and body size scaling

Robusticity index The two allometric regressions between L and $V^{1/3}$ are significant ($p < 0.001$; Table 6), but the PGLS regression indicates slight negative allometry, whereas the major axis regression does not allow us to exclude isometry. This suggests that the canal robusticity index $L/V^{1/3}$ is only slightly affected by intrinsic size-scaling effects, i.e., that carotid canal length and volume covary in an almost linear fashion when geometric similarity is considered. This is further confirmed by the lack of significant correlation between $L/V^{1/3}$ against CS (Table 6). When separate allometric regressions of L and $V^{1/3}$ against CS are computed, it emerges that $V^{1/3}$ and CS display an isometric relationship, whereas L and CS display a minimally positive allometric relationship (with a slope very close to 1). Overall, this suggests that these three variables are suitable proxies for the size of the carotid canal and that the robusticity index is only very slightly affected, if at all, by intrinsic size-scaling effects related to the overall size of the canal.

Based on the robusticity index, and despite some overlap, platyrrhines display significantly slenderer canals than catarrhine families, while hominids also display slenderer canals than both cercopithecids and hylobatids, with the latter showing the stoutest canals (Fig. 5c; Table 3; SOM Tables S3 and S4). *Ekembo* and *Epipliopithecus* exhibit similar indices, while *Victoriapithecus* shows a somewhat higher value but similarly overlaps with all

catarrhine families (Fig. 5c; Table 4), and *Pliobates* shows an even higher value and falls outside the hylobatid range (Fig. 5c; Table 4). However, none of the fossil specimens significantly differs from any extant clade (Table 5).

Body-size allometry The fact that the robusticity index is not markedly affected by the size of the canal itself notwithstanding, either carotid canal size and/or proportions could still be affected by body size-scaling effects as measured by regressions against BM (Table 6). Both L and CS display a negative allometric relationship relative to BM—slightly below the theoretical isometric slope of 1/3 predicted by geometric similarity—whereas, in contrast, $V^{1/3}$ fits well with the prediction of geometric isometry. This suggests that the volume of the carotid canal is a better proxy for BM than either L or CS if size-scaling effects are not corrected for, because the former variable is directly proportional to BM in a linear fashion, whereas both L and CS display negative allometry relative to BM. The similar allometric pattern of L and CS is not surprising, because the latter was computed from the carotid canal configurations—which are sets of canal streampoints—and, hence, it only contains information about carotid canal length (but not volume).

Differences in size scaling between L and V are reflected in the existence of a mild negatively allometric relationship when L is considered the dependent variable, although such a relationship is not significant when both variables are considered to display error (i.e., isometry cannot be excluded in the major axis regression; Table 6). Differences in scaling between L and V relative BM, in any case, are reflected in the regression between the robusticity index and BM (Table 6), which is of inverse proportionality (i.e., a negative slope): since the numerator (L) of the index increases slightly slower than the denominator ($V^{1/3}$) relative to BM, the index tends to decrease as the body size increases. However, it is

454 noteworthy that despite being significant, the correlation between the robusticity index and
455 body size only explains 14% of the variance (Table 6).
456
457 *3.3. Carotid canal course within the petrosal*
458 Principal components analysis The bgPCA discriminates between platyrrhines and
459 catarrhines but not among catarrhine families (Fig. 6). The cross-validated bgPCA (SOM Fig.
460 S3) is virtually identical to the standard bgPCA, and the permutational ANOVA results (SOM
461 Table S5) show that mean group differences are significant in all instances. The percentage
462 of variance explained by bgPCAs only increases slightly as compared with the raw data—
463 indicating that grouping structure is not spurious. The percentage of correctly classified
464 individuals by the bgPCA (Table 7) is moderately high (79%), even after cross-validation
465 (77%), although much higher in the case of platyrrhines (92%) and hominids (91%) than for
466 cercopithecoids (63%) and hylobatids (64%).
467 bgPC1 (Fig. 6a) explains most of the variance (94%), is not significantly correlated with CS
468 (p = 0.21; Table 6), and shows a strong phylogenetic signal at $p < 0.001$ ($\lambda = 0.95$; $K = 3.28$).
469 Although bgPC1 is not significantly correlated to ln CS, it displays significant allometry
470 relative to both $V^{1/3}$ and BM, but only explains 19% and 25% of the shape variance,
471 respectively (Table 6). This axis discriminates platyrrhines (negative scores) from catarrhines
472 (positive scores) at $p < 0.001$ (Fig. 5d; Table 3; SOM Tables S3 and S4) because of longer
473 canals that originate more inferolaterally in the petrosal of the former (Figs. 6b, 7; SOM Figs.
474 S4–S6). In contrast, catarrhines display shorter canals that originate more superiorly and are
475 overall located more medially in the petrosal (Figs. 6b and 7; SOM Figs. S4–S6). Extant
476 catarrhine families extensively overlap along bgPC1 and do not significantly differ in terms of
477 canal length and foramen/canal superoinferior and mediolateral position (Fig. 5d; Table 3;

SOM Tables S3 and S4). *Pliobates* and the remaining fossil taxa display similar (moderately negative) bgPC1 scores that are intermediate between those of extant catarrhines and extant platyrrhines (Figs. 5d and 6a; Table 4) and only slightly overlap with cercopithecids and hominids or, in the case of *Epipliopithecus*, also marginally with platyrrhines. Their canal configuration (SOM Figs. S4–S6) is thus somewhat shorter and more medially located than in platyrrhines, although *Epipliopithecus* more closely resembles the platyrrhine condition than *Pliobates*, *Victoriapithecus*, and *Ekembo* do.

bgPC2 (Fig. 6a) explains only 5% of variance, is significantly correlated with CS, $V^{1/3}$, and BM (explaining respectively 58%, 46%, and 35% of the shape variance; Table 6), and shows significant phylogenetic signal at $p < 0.001$ ($\lambda = 0.99$; $K = 0.62$). Variation along bgPC2 (Figs. 6b, 7) reflects the canal position on the petrosal (more anterior toward negative values, and more posterior toward positive scores). Platyrrhines and catarrhines extensively overlap along this axis, but hominids display significantly more positive values than other groups despite considerable overlap (Fig. 5e; SOM Figs. S4–S6; SOM Tables S3 and S4). Along bgPC2, *Epipliopithecus*, *Victoriapithecus* and *Ekembo* are found on slightly negative scores and overlap with platyrrhines, cercopithecids and hylobatids, whereas *Pliobates* has a slightly positive score that further overlaps with hominids (Figs. 5e and 6a; Table 4). The canal configuration of *Pliobates* is thus somewhat more posteriorly located than in the other extinct taxa (SOM Figs. S4–S6), particularly *Epipliopithecus*.

Z-scores (Table 5) indicate that, for bgPC1, *Epipliopithecus* significantly differs from all extant groups, while other extinct taxa match the hominid distribution only. In contrast, for bgPC2, *Epipliopithecus*, *Victoriapithecus* and *Ekembo* only significantly differ from hominids, whereas *Pliobates* matches the variation of the four extant groups. When both bgPCs are considered simultaneously, the analyzed extinct taxa differ from the four extant anthropoid

groups except for *Pliobates*, which matches the hominid variation. This is confirmed by posterior probabilities of group membership (Table 8), according to which *Epipliopithecus*, *Victoriapithecus*, and *Ekembo* are classified as cercopithecoids—although *Epipliopithecus* falls outside their range of variation ($p = 0.018$)—whereas *Pliobates* is classified as a hominid and only significantly differs from platyrrhines. According to these results, the canal course of both *Ekembo* and *Victoriapithecus* fit better the cercopithecoid variation, whereas *Pliobates* fits better with hominids, and *Epipliopithecus* does not fit well with any of the extant groups analyzed. This notwithstanding, the results of the NJ cluster analysis (Fig. 8) indicate that *Pliobates* and *Epipliopithecus* are most similar to one another. Indeed, the four analyzed extinct taxa are grouped together in a cluster of their own, distinct from the subcluster of great apes and that of platyrrhines.

The discrimination among the catarrhine families in the catarrhine-only bgPCA is slightly better than in the analysis based on the whole sample but the three groups still overlap to an important extent (SOM Fig. S7). The first axis explains most of the variance (85.33%) and is the only one that discriminates between hominids and the remaining groups—as in the whole sample analysis, in which only one axis (bgPC2) discriminates between them. The results for the fossils in the catarrhine-only analysis are not more conclusive than for the analysis including platyrrhines, with only minor differences. In particular, *Epipliopithecus* falls closer to the hylobatid centroid and is classified as a hylobatid ($p = 0.54$), although it displays no significant differences with either cercopithecids ($p = 0.30$) or hominids ($p = 0.29$); *Victoriapithecus* still matches better the cercopithecid range of variation ($p = 0.22$), as it is the case for *Ekembo* ($p = 0.73$), while *Pliobates* is classified first as a hominid ($p = 0.39$) but also falls within the range of hylobatids ($p = 0.14$)—apparently owing to the more hominid-like condition of *Symphalangus* as compared to other hylobatids.

Phylomorphospace The results of the phylomorphospace (Fig. 9; SOM Fig. S8) and the reconstructed ancestral morphotypes (Fig. 10; SOM Fig. S9) are virtually identical irrespective of the hypothesis considered. The crown platyrrhine LCA displays a very long canal that originates inferiorly and is located very laterally in the petrosal (Fig. 10e; SOM Fig. S9e), whereas the crown catarrhine LCA displays a condition almost indistinguishable from the mean anthropoid configuration (Fig. 10f; SOM Fig. S9f). The inferred crown cercopithecoid (Fig. 10g; SOM Fig. S9g) and crown hominoid (Fig. 10h; SOM Fig. S9h) ancestral morphotypes are not very divergent from one another or from the catarrhine LCA, but both are more derived than the latter by displaying a somewhat shorter and more medially and posteriorly located canal. The crown hylobatid (Fig. 10i; SOM Fig. S9i) and crown hominid (Fig. 10j; SOM Fig. S9j) LCAs more clearly diverge from the crown hominoid LCA in different directions. Thus, the hylobatid LCA displays a higher bgPC1 score overlapping with extant hylobatids and cercopithecoids, due to a shorter and more medially located canal. In contrast, the hominid LCA displays a higher bgPC2 than the crown hominoid LCA (like the extant hylobatid *Symphalangus*) due to a more posteriorly located canal.

The four analyzed extinct taxa are broadly similar to the crown catarrhine LCA's condition (Fig. 9). Indeed, both *Victoriapithecus* (Fig. 10d) and *Ekembo* (Fig. 10c) most closely resemble the crown catarrhine LCA rather than the crown ceropithecoid (Fig. 10g) or hominoid (Fig. 10h) LCAs. *Epipliopithecus* (Fig. 8b) displays a slightly more platyrrhine-like condition in bgPC1 but is nevertheless very distinct from the crown platyrrhine LCA (Fig. 10e) and closer to the inferred crown catarrhine ancestral condition. *Pliobates* (Fig. 10a) closely resembles the crown catarrhine LCA in canal length and carotid foramen/canal superoinferior and mediolateral position (as reflected in bgPC1), but unlike *Victoriapithecus* and *Ekembo* it appears derived along bgPC2 toward the reconstructed ancestral hominid condition—albeit

being more similar along this axis to *Symphalangus* than to extant great apes—due to its more posteriorly located canal.

4. Discussion

4.1. Carotid canal orientation

Two different characters were defined by Alba et al. (2015b: Tables S5 and S6) to code the carotid canal morphology, one describing the canal 'orientation' (more or less horizontal) and another (following Shoshani et al., 1996) describing the canal 'direction' (more or less anterior). In Alba et al. (2015b), canal 'orientation' was defined as the inclination between the canal and the basioccipital, whereas canal 'direction' was coded based on the spatial relationship between the imaginary line emerging from the canal and the foramen magnum. Canal 'direction' sensu Alba et al. (2015b) could be anterior or posterior relative to the foramen magnum, i.e., more laterally or more anteriorly directed, respectively. To evaluate this character, previous authors (Shoshani et al., 1996) placed a straight wire inside the carotid canal and noted the point of intersection between the imaginary line along the wire and the foramen magnum. In Alba et al. (2015b) on the other hand, this character was evaluated conducting visual inspections on μCT scans, drawing the course of the canal on basicranium inferior view and noting the point of intersection between the imaginary line in continuation of the canal course and the foramen magnum. 2DYZA (canal superior orientation in the present study) is comparable with Alba et al.'s (2015b) canal 'orientation' because this angle is measured along the parasagittal plan, although based on values obtained we prefer to categorize them as oblique/subvertical/vertical (as opposed to horizontal/oblique/subvertical as in Alba et al., 2015b). In contrast, 2DXYA (canal medial orientation in the present study) is not directly

574 comparable with Alba et al.'s (2015b) canal 'direction', because while both studies rely
575 primarily on the line passing through the two canal endpoints (i.e., whole carotid canal), in
576 the present study the alignment process and the quantitative assessment of this character
577 (i.e., possibility of having more than two states vs. two qualitative states only in Alba et al.
578 [2015b]) make that this measure of canal orientation, for a same canal specimen, might
579 differ between the two studies.

580 *Pliobates* was coded by Alba et al. (2015b) as displaying a horizontal orientation
581 parallel to the basioccipital, like hylobatids, whereas the stem catarrhine *Saadanius*,
582 cercopithecoids (including *Victoriapithecus*) and hominids were coded with a subvertical
583 orientation, and *Epipliopithecus* and *Ekembo* with an intermediate (oblique) condition. Our
584 results for superior canal orientation (2DYZA) indicate that, in this regard, *Pliobates* does not
585 differ from hylobatids and display a lower value than *Ekembo* and *Epipliopithecus*. However,
586 our results further show that both hylobatids and hominids display a rather oblique
587 orientation (i.e., a horizontal orientation parallel to the basioccipital using the terminology of
588 Alba et al., 2015b), with *Ekembo* and *Epipliopithecus* resembling hominoids as a whole.
589 Nonetheless, all these taxa possess a less vertical orientation than platyrrhines (i.e., a
590 subvertical canal) and, especially, cercopithecoids (including *Victoriapithecus*), in which the
591 canal is vertical. To sum up, according to Alba et al. (2015b) hylobatids and *Pliobates* had a
592 horizontal canal, *Ekembo* and *Epipliopithecus* an oblique canal, and cercopithecoids
593 (including *Victoriapithecus*) and hominids a subvertical canal, whereas according to our
594 results all hominoids (including *Ekembo*), *Epipliopithecus*, and *Pliobates* have an oblique
595 canal, platyrrhines a subvertical canal, and cercopithecoids (including *Victoriapithecus*) an
596 even more vertical canal. Therefore, the superior orientation of the carotid canal is

consistent with the cercopithecoid status of *Victoriapithecus*, but it is not informative regarding the stem catarrhine vs. stem hominoid status of *Pliobates*.

In turn, *Pliobates* was coded by Alba et al. (2015b) as resembling *Epipliopithecus* and hylobatids in the 'direction' of the canal. The condition of all these taxa was coded as anteriorly directed, the imaginary line emerging from the carotid canal crossing the foramen magnum more posteriorly than in *Saadanius*, cercopithecids, and hominids, whose canal would be more laterally directed, as in platyrrhines (see also Shoshani et al., 1996). In contrast, our results indicate that hylobatids extensively overlap in canal medial orientation with other extant catarrhines, which only significantly differ from platyrrhines. Furthermore, *Pliobates* does not specifically resemble hylobatids or *Epipliopithecus*, but rather crown catarrhines as a whole, including *Victoriapithecus*. On the other hand, *Epipliopithecus* and, especially, *Ekembo,* exhibit a more platyrrhine-like condition, i.e., a medially directed canal. To sum up, our results indicate that cercopithecoids (including *Victoriapithecus*), crown hominoids, and *Pliobates* have an anteriorly oriented canal, whereas platyrrhines, *Ekembo*, and *Epipliopithecus* have a medially oriented canal.

4.2. Carotid canal proportions

Volumetric proportions—which were not considered by Alba et al. (2015b)—as measured by the robusticity index of the carotid canal, further confirm the differences in carotid canal morphology between platyrrhines and catarrhines. Our allometric analyses indicate that these differences cannot be explained by body size-scaling effects alone. In particular, the volume of the carotid canal displays an isometric relationships with body size, whereas length displays a slight negative allometric relationship with the latter. As a result, larger-bodied taxa tend to display lower values of the robusticity index (i.e., slightly stouter

carotid canals). However, correlation with body mass only explains 14% of the variance in carotid canal robusticity.

Based on our results, platyrrhines display on average slenderer canals (i.e., lesser volume relative to length) than catarrhines. However, as for medial canal orientation, catarrhine families largely overlap in canal proportions, although great apes display less robust canals than cercopithecids and hylobatids, and are somewhat intermediate between them and platyrrhines. The analyzed fossil catarrhines more closely resemble each other in canal proportions than in canal orientation—being catarrhine-like but further overlapping with the platyrrhine range of variation. *Pliobates* displays somewhat slenderer canals than the other extinct taxa and, unlike them, it does not overlap with the hylobatids, even more clearly than in the case of medial canal orientation thus further reinforcing the rejection of possible closer similarities with hylobatids the latter family.

Our results for the extant taxa are in broad agreement with those previously obtained by Boyer et al. (2016) on relative internal carotid artery area. Boyer et al. (2016) found internal carotid area to scale isometrically with cranial area (measured as the square root of the product between prosthion-inion length and bizygomatic breadth). Among catarrhines, these authors found a pattern of decreasing robusticity in relative carotid artery area from hylobatids to hominids, and to cercopithecids, which is the same as we found for the carotid canal as a whole. The main difference between our results and those of Boyer et al. (2016) is that, in the latter study, the carotid artery robusticity of platyrrhines was found to be intermediate between hylobatids and hominids, whereas our results show that platyrrhines have slenderer canals than catarrhines. This discrepancy is easily explained by the fact that Boyer et al. (2016) considered internal carotid artery area relative to cranial area, whereas we relied on the ratio between the length and the volume of the canal. Our results (see

below for further discussion) indicate that platyrrhines display relatively longer carotid canals than catarrhines, thereby resulting in less robust volumetric proportions for the canal as a whole. Given that Boyer et al. (2016) did not took canal length into account, this explained the above-mentioned discrepancy for platyrrhines (but not the other groups) as compared to our results.

4.3. Carotid canal course

Our bgPCA results indicate that the morphology of the canal embeds strong phylogenetic signal, although most of the variance merely discriminates between platyrrhines and catarrhines, due to differences in canal length and location reflected in bgPC1. In particular, extant catarrhines display shorter canals that originate more superiorly than in platyrrhines. It is noteworthy to stress beforehand that *Pliobates* and hylobatids do not show particular similarities in bgPC1 scores.

Previous studies suggested that the carotid foramen is located ventrally (Ross, 1994; Ross et al., 1998) and posteriorly (Ross, 1994; Ross et al., 1998; Kay et al., 2008) in both platyrrhines and catarrhines, whereas Alba et al. (2015b) noted some differences in the anteroposterior carotid foramen location between hylobatids and other catarrhines (with the former displaying a more anteriorly located carotid foramen). Previous studies also noted that platyrrhines display a more medially located foramen than catarrhines (Ross et al., 1998; Kay et al., 2008). Our bgPC1 results indicate that extant platyrrhines and catarrhines differ not only regarding the length of the canal, but also the location of the (external) carotid foramen, such that in catarrhines the entire carotid canal (i.e., not only the foramen but the whole structure) is more superiorly and medially located within the petrosal. Our results therefore point to differences between platyrrhines and catarrhines in

terms of dorsoventral location of the carotid foramen, contrary to previous studies (Ross, 1994; Ross et al., 1998). This might be attributable to the different methodologies employed (i.e., because of having performed an alignment on the specimens in the present study). Similarly, because of the alignment, our conclusions for the location along the mediolateral axis might be the opposite as those noted by previous authors (Ross et al., 1998; Kay et al., 2008), who simply recorded foramen position relative to the bulla. Since catarrhines possess a tubular ectotympanic, catarrhine landmark configurations are shifted more medially. This is the consequence of alignment optimization of their tympanic landmarks with those of platyrrhines, whose annular ectotympanic causes their tympanic landmarks to be more medially positioned. Regardless, we observe an extensive overlap among extant catarrhine families in the position of the carotid foramen, at least based on bgPC1.

Our results for bgPC2 lend some support that hylobatids display on average a more anteriorly located foramen in the petrosal than hominids. However, rather than indicating a particular condition for hylobatids, our bgPC2 results suggest that only hominids differ in this regard from other catarrhines by displaying a more posteriorly located foramen. This conclusion should be taken with caution, given that bgPC2 shows an extensive overlap between hominids and the upper range of other crown catarrhines. Furthermore, bgPC2 reflects a smaller amount of variance, embeds lesser phylogenetic signal than bgPC1, and is more strongly correlated with size—although the percentage of variance explained by allometry varies depending on whether canal size or body size is considered, our results clearly indicate that this axis is more strongly influenced by size-scaling than bgPC1. Therefore, one should be cautious when interpreting similarities among taxa based on bgPC2 scores.

Our 3DGM results for the analyzed fossil taxa do not support particular similarities between *Pliobates* and hylobatids in terms of overall carotid canal course (contra Alba et al., 2015b), and indicate instead that *Pliobates* is most similar in this regard to *Epipliopithecus*, *Victoriapithecus* and *Ekembo*. All these fossil catarrhines appear overall closer to extant catarrhines in terms of canal length and location in the petrosal, albeit being somewhat intermediate between platyrrhines and catarrhines. *Epipliopithecus* appears slightly more platyrrhine-like, whereas the other extinct genera only overlap with the lowest range of cercopithecids and hominids (but not hylobatids). *Pliobates* only differs slightly from the remaining fossil catarrhines by more closely resembling hominids and *Symphalangus* along bgPC2 (reflecting a more posteriorly located foramen/canal). As noted above, bgPC2 is quite strongly correlated with CS, suggesting that the differences between hominids and the rest of the sample could merely result from the larger body size of the former. However, this cannot explain the differences along this axis between *Pliobates* and *Epipliopithecus*, as the former more closely resembles the large-bodied hominids and the largest-bodied hylobatid (*Symphalangus*) despite a much lower estimated body size than *Epipliopithecus* (4–5 kg vs. 11–12 kg, respectively; Alba et al., 2015b).

4.4. Evolutionary implications

Alba et al. (2015b) concluded that *Pliobates* displays a mosaic of plesiomorphic (stem catarrhine-like) cranial and postcranial features and more derived (crown hominoid) cranial and postcranial synapomorphies, coupled with a dendropithecid-like dentition and some cranial similarities with hylobatids. A stem hominoid status more derived than that of *Ekembo* was supported for *Pliobates* by Alba et al. (2015b) based on the results of their

715 cladistic analysis. Such a phylogenetic placement would support the view that some
716 purported synapomorphies of crown catarrhines, best exemplified by the completely
717 ossified tubular ectotympanic, would have been independently acquired independently in
718 cercopithecoids and hominoids—a possibility taken into account by some previous authors
719 (Begun, 2002). A stem hominoid status for *Pliobates* would further support that the last
720 common ancestor of crown hominoids would have been more hylobatid-like than previously
721 assumed (Alba et al., 2015b). Interestingly, one of the resemblances between *Pliobates* and
722 hylobatids found by Alba et al. (2015b) was the carotid canal morphology, which is at odds
723 with the results of our more elaborate analyses of this anatomical structure, which denote a
724 generalized catarrhine morphology with some closer similarities with extant hominids and
725 uniquely *Symphalangus* among hylobatids.

726 Contrary to Alba et al. (2015b), subsequent cladistic analyses–based on different taxon-
727 character matrix–have recovered *Pliobates* as a stem catarrhine more closely related to
728 pliopithecoids (Nengo et al., 2017; Gilbert et al., 2020b). Based on these results, Gilbert et al.
729 (2020a: 399) concluded that "*Pliobates* is most likely a derived, late-occurring pliopithecoid
730 or other stem catarrhine taxon that has converged on some interesting but minor details of
731 extant hominoid elbows and wrists". In fact, the similarities in elbow and wrist morphology
732 between *Pliobates* and hominoids are not minor but quite extensive, more so than those
733 displayed by *Ekembo* and certainly than those convergently acquired by atelids (Alba et al.,
734 2015b). However, it is not unconceivable that these similarities—being functionally related
735 to enhanced forearm rotation and ulnar deviation capabilities—might have independently
736 evolved between *Pliobates* and crown hominoids. Under such scenario, in which postcranial
737 similarities between *Pliobates* and crown hominoids would be dismissed as convergences, it
738 should be taken into account that the dental morphology of *Pliobates* suggests much closer

739 affinities to dendropithecids (particularly *Micropithecus*) than to pliopithecoids (Alba et al.,
740 2015b). A dendropithecid status for *Pliobates* would not imply an independent acquisition of
741 a fully-ossified ectotympanic, but would not automatically resolve the phylogenetic
742 placement of the former, given the controversies surrounding the phylogenetic relationships
743 of dendropithecids—considered either stem catarrhines more derived than pliopithecoids
744 (Harrison, 2010, 2013, 2017; Nengo et al., 2017; Gilbert et al., 2020b) or stem hominoids
745 more basal than proconsulids (Rae, 1999; Zalmout et al., 2010; Begun, 2015; Alba et al.,
746 2015b; Rossie and Hill, 2018).

747 Unfortunately, the carotid canal morphology of dendropithecids is currently unknown,
748 thereby precluding a direct comparison with *Pliobates*. Furthermore, despite substantial
749 differences between platyrrhines and catarrhines in terms of carotid canal orientation and
750 proportions as well as carotid canal length and (foramen) location in the petrosal, our results
751 indicate a considerable overlap among extant catarrhines. As a result, carotid canal
752 morphology is of limited utility for investigating the phylogenetic position of fossil
753 catarrhines, although some insights can be drawn for the investigated taxa. Before
754 discussing the evolutionary implications of our results, however, it should be noted that the
755 small sample sizes available for extinct taxa make it necessary interpret the differences
756 among the analyzed fossil specimens by assuming that they are more or less representative
757 of their respective taxa. Although this caveat is not restricted to the carotid canal
758 morphology, it should not be forgotten that we cannot know a priori how similar in carotid
759 canal morphology a particular fossil specimen is to the (unknown) average condition of the
760 taxon to which it belongs. For example, given the considerable variation that can be
761 observed in some extant taxa for carotid canal course (e.g., *Aotus*, *Macaca*, *Mandrillus*), the
762 possibility remains that some of the differences inferred among extinct taxa, or between

them and extant catarrhine clades, might vanish (or become more accentuated) if additional specimens became available. In the meantime, caution is required by bearing in mind that the reliability of inferences for fossil taxa is limited by the number of specimens available to them, which often preclude an adequate assessment of intraspecific variability.

Based on the currently available specimens, our results indicate that the stem hominoid *Ekembo* and the stem cercopithecoid *Victoriapithecus* are virtually identical in carotid canal volumetric proportions and course morphology, although *Ekembo* displays a more platyrrhine-like medial orientation (like *Epipliopithecus*) and a more hominoid-like superior orientation (like *Epipliopithecus* and *Pliobates* to some extent). The less medially/more anteriorly oriented carotid canal in *Pliobates* than in *Ekembo* would be consistent with a more derived stem hominoid status, but given the modern cercopithecoid-like carotid canal orientation of *Victoriapithecus*, the condition of extant cercopithecoids and hominoids might have evolved independently to some extent. In turn, based on the condition of *Epipliopithecus*, the possession of an obliquely oriented canal in hominoids might represent a catarrhine symplesiomorphy; in that case, the condition of extant cercopithecoids would have independently evolved from that of extant platyrrhines. Alternatively, the oblique orientation of the canal might be synapomorphic for hominoids, in which case the similar condition of *Epipliopithecus* would be a convergence. Either way, this feature is not informative regarding the phylogenetic position of *Pliobates*.

In terms of carotid canal course, as reflected by our 3DGM analysis, *Pliobates* does not show particular affinities with hylobatids, and rather resembles the other analyzed extinct taxa, which are overall more similar to catarrhines but somewhat intermediate between platyrrhines and both cercopithecids and hominids. The phylomorphospace shows that both

Victoriapithecus and *Ekembo* apparently reflect well the inferred ancestral crown catarrhine morphotype, despite their generally accepted crown catarrhine (respectively, stem cercopithecoid and stem hominoid) status (e.g., Benefit and McCrossin, 1997; Benefit, 1999; Alba et al., 2015b; Nengo et al., 2017; Gilbert et al., 2020b). In contrast, *Epipliopithecus* appears somewhat more plesiomorphic, whereas *Pliobates* appears slightly derived (in the anteroposterior position of the carotid foramen/canal) toward the great ape condition, being closer to the inferred ancestral hominid morphotype as well as the hylobatid *Symphalangus*.

In the case of *Epipliopithecus*, our results are in agreement with the widely held opinion that pliopithecoids are a clade of stem catarrhines, predating the divergence of cercopithecoids and hominoids (Harrison, 2013; Begun, 2002, 2017; Nengo et al., 2017; Gilbert et al., 2020a, b; Sankhyan et al., 2017; Harrison et al., 2020; Urciuoli et al., 2021; contra Alba et al., 2015b). For *Pliobates*, our results are more ambiguous and subject to interpretation, although it is noteworthy that they do not support a closer relationship with pliopithecoids–at least, based on the information provided by *Epipliopithecus*. They suggest instead that, in carotid canal morphology, *Pliobates* is more derived than *Epipliopithecus* toward the inferred ancestral crown catarrhine morphotype, like *Ekembo* and *Victoriapithecus*. Furthermore, our results discount very close similarities in carotid canal morphology between *Pliobates* and hylobatids as a whole, but indicate some resemblances with the hylobatid *Symphalangus* and great apes. In the latter regard, *Pliobates* is approximately equidistant from the crown catarrhine and crown hominoid reconstructed morphotypes. It is uncertain whether this reflects a more derived status of *Pliobates* or an independent development, although the latter is plausible in light of the *Symphalangus* condition—if the hylobatid LCA reconstructed in the phylomorphospace is broadly correct,

Symphalangus must have independently acquired a more great ape-like condition; alternatively, the condition shared by the hominid LCA and *Symphalangus* might be plesiomorphic for crown hominoids and the reconstructed hylobatid LCA would reflect a secondary reversal of the remaining hylobatids. Of course, the morphology of a single anatomical region cannot provide much insight on the phylogenetic position of a given taxon among catarrhines, particularly if—as it is the case of the carotid canal—it does not adequately discriminate among catarrhine clades. However, our results for this structure do not show any particular resemblances between pliopithecoids and *Pliobates* (beyond those displayed by all the extinct taxa analyzed), and further fail to contradict the alternative phylogenetic status of *Pliobates* as a stem hominoid. The phylogenetic status of *Pliobates* thus seems far from being settled.

5. Summary and conclusions

Previous research on the primate carotid canal within a phylogenetic context has been limited to the inclusion of qualitative features related to carotid foramen position in the bulla and overall direction and orientation of the canal itself in character-taxon matrices devised for cladistic analysis (Beard and MacPhee, 1994; Ross, 1994; Shoshani et al., 1996; Ross et al., 1998; Kay et al., 2008; Alba et al., 2015b). From a quantitative viewpoint, only Boyer et al. (2016) investigated the allometric relationship between carotid canal area and BM (Boyer et al., 2016), whereas some authors relied on carotid canal area for inferring encephalic blood flow rates and blood flow metabolism by further taking vertebral canal size into account (Boyer and Harrington, 2018, 2019; Beaudet et al., 2020). Thus, our study is the first to rigorously quantify the orientation, direction, overall course and volumetric

proportions of the carotid canal in 3D among a large sample of anthropoids. The allometric regressions performed also represent an advancement in the understanding of body size-scaling effects on carotid canal morphology. The methodological protocols devised here enable repeatability among different researchers and thus will enable a refinement of our conclusions by adding additional extant and fossil specimens in the future. The analyzed variables are no panacea for clarifying the phylogeny of extinct catarrhines, because various extant groups overlap to a large extent and also because intraspecific variation will be difficult to evaluate due to small samples sizes. However, the analyzed variables offer the prospect to provide taxonomically and phylogenetically relevant information for extinct taxa, particularly if they are added to character-taxon matrices devised for cladistic analysis including information from other anatomical areas. Other future directions of work on the carotid canal should deepen our current understanding about the influence of function, as well as allometric and phylogenetic constraints, on the evolution of this anatomical structure. This would be required not only to better interpret carotid canal morphology from an adaptive viewpoint, but also to derive from it paleobiological inferences for extinct taxa.

In this study, we rely on 3D morphometric techniques to quantify the orientation, proportions, and course of the carotid canal in the small-bodied catarrhine *Pliobate*s, and compare it with extant anthropoids and other Miocene catarrhines (*Epipliopithecus*, *Victoriapithecus,* and *Ekembo*). Our results reveal that *Pliobates* and the other analyzed Miocene catarrhines are broadly similar to one another in carotid canal morphology and more closely resemble extant catarrhines than platyrrhines. Unfortunately, carotid canal morphology does not adequately discriminate among catarrhine clades, thereby hindering a more detailed phylogenetic assessment of *Pliobates* on this basis. The difficulty of assessing intraspecific variation in carotid canal morphology in the extinct taxa, coupled with the lack

of marked differences among extant catarrhine families, make it impossible to reach definitive conclusions about the systematic position of *Pliobates* on this basis alone. However, our results rule out the previously noted similarities in carotid canal morphology between *Pliobates* and hylobatids and indicate instead that this extinct catarrhine is broadly similar to catarrhines as a whole and, in particular, to other Miocene catarrhines (both stem and crown).

It is however noteworthy that the carotid canal of *Pliobates* is not particularly similar to that of pliopithecoids (as represented by *Epiplioithecus*, which appears somewhat more platyrrhine-like), thereby not supporting (or contradicting) the hypothesis that *Pliobates* is a pliopithecoid. Like the stem hominoid *Ekembo* and the stem cercopithecoid *Victoriapithecus*, *Pliobates* appears somewhat more derived than *Epipliopithecus* toward the modern catarrhine condition, and indeed, in some respects, *Pliobates* appears even more derived toward the ancestral hominoid morphotype than the remaining Miocene catarrhines analyzed, more closely resembling extant hominids and the hylobatid *Symphalangus*. Therefore, our results do not enable us to discount the hypothesis that *Pliobates* is a stem hominoid rather than a stem catarrhine. Given the dental similarities between *Pliobates* and African dendropithecids, the former might be a late offshot of the latter clade that dispersed into Eurasia independently from pliopithecoids. Unfortunately, this possibility could not be directly assessed in this study because the carotid canal morphology of dendropithecids is unknown. Additional analyses focused on other anatomical (both cranial and postcranial) areas will be required to further clarify the phylogenetic relationships of *Pliobates*, as well as to clarify whether its postcranial similarities with crown hominoids might have been independently acquired.

880

881 **Acknowledgments**

882 This work has been funded by the Agencia Estatal de Investigación (CGL2016-76431-P and
883 CGL2017-82654-P, AEI/FEDER, EU), the Generalitat de Catalunya (CERCA Programme and
884 Consolidated Research Groups 2017 SGR 086 and 2017 SGR 116), the Ministerio de Ciencia,
885 Innovación y Universidades (PRE2018-083299 to F.B. and BES-2015–071318 to A.U.), and the
886 European Commission under the Marie Skłodowska-Curie Individual Fellowship Programme
887 (H2020-MSCA-IF-2018-837966 to M.P.). A.B. was funded by the Centre of Excellence in
888 Palaeosciences (CoE-Pal), Institut français d'Afrique du Sud (IFAS), National Research
889 Foundation (NRF), Palaeontological Scientific Trust (PAST), and Wits. Regarding the CT
890 scanning of *Epipliopithecus*, this research also received support from the Synthesys Project
891 (http://synthesys3.myspecies.info/), which is financed by the European Community
892 Research Infrastructure Action under the FP7 (ref. AT-TAF-4689). We thank Fred Spoor, the
893 Department of Earth Sciences of the National Museums of Kenya, and the Department of
894 Human Evolution of the Max Planck Institute for Evolutionary Anthropology in Lepzig for
895 granting access to the CT scans of *Ekembo* and *Victoriapithecus,* as well as Ursula Göhlich for
896 access to the *Epipliopithecus* material housed in the Naturhistorisches Museum Wien and
897 Martin Dockner for assistance during the CT scanning process of this material at the µCT lab
898 of Universität Wien. We also thank the following people and institutions for providing access
899 to scans used in this study: Eric Delson and the American Museum of Natural History
900 (AMNH), funded by the AMNH and the New York Consortium in Evolutionary Primatology
901 (NYCEP); Lauren A. Gonzales, the Museum of Comparative Zoology (MCZ), the Southern
902 Illinois University (SIU), and the Smithsonian National Museum of Natural History (USNM),
903 funded by NSF grants BCS 1440742 & 1552848; Kari L. Allen and the Duke University,

Department of Evolutionary Anthropology (DUEA), regarding scans that originally appeared in Allen's PhD dissertation, funded by an NSF DDIG and the Leakey Foundation; Lynn Copes, Lynn Lucas, and the MCZ, funded by an NSF DDIG #0925793 and the Wenner Gren Foundation; and Sergio Almécija, funded by NSF grant BCS 1316947 and Stony Brook University. These scans were downloaded from MorphoSource.org, a web-accessible archive for 3D digital data housed by Duke University. We further thank the Editor (Clément Zanolli), the Associate Editor (Eric Delson), and three anonymous reviewers for helpful comments that helped us to improve a previous version of this paper.

References

Adams, D.C., Collyer, M.L., Kaliontzopoulou, A., 2019. Geomorph: Software for geometric morphometric analyses. R Package Version 3.3.1. https://cran.r-project.org/web/packages/geomorph/index.html.

Alba, D.M., Delson, E., Carnevale, G., Colombero, S., Delfino, M., Giuntelli, P., Pavia, M., Pavia, G., 2014a. First joint record of *Mesopithecus* and cf. *Macaca* in the Miocene of Europe. J. Hum. Evol. 67, 1–18.

Alba, D.M., Colombero, S., Delfino, M., Martínez-Navarro, B., Pavia, M., Rook, L., 2014b. A thorny question: The taxonomic identity of the Pirro Nord cervical vertebrae revisited. J. Hum. Evol. 76, 92–106.

Alba, D.M., Montoya, P., Pina, M., Rook, L., Abella, J., Morales, J., Delson, E., 2015a. First record of *Mesopithecus* (Cercopithecidae, Colobinae) from the Miocene of the Iberian Peninsula. J. Hum. Evol. 88, 1–14.

926 Alba, D.M., Almécija, S., DeMiguel, D., Fortuny, J., Pérez de los Ríos, M., Pina, M., Robles,
927 J.M., Moyà-Solà, S., 2015b. Miocene small-bodied ape from Eurasia sheds light on
928 hominoid evolution. Science 350, aab2625.
929 Arnold, C., Matthews, L.J., Nunn, C.L., 2010. The 10kTrees website: A new online resource for
930 primate phylogeny. Evol. Anthropol. 19, 114–118.
931 Barry, J.C., Jacobs, L.L., Kelley, J., 1987. An early middle Miocene catarrhine from Pakistan
932 with comments on the dispersal of catarrhines into Eurasia. J. Hum. Evol. 15, 501–508.
933 Beard, K.C., MacPhee, R.D.E. 1994. Cranial anatomy of *Shoshonius* and the antiquity of
934 Anthropoidea. In: Fleagle, J.G., Kay, R.F. (Eds.), Anthropoid Origins. Plenum Press, New
935 York, pp. 55–97.
936 Beaudet, A., Clarke, R.J., Heaton, J.L., Pickering, T.R., Carlson, K.J., Crompton, R.H.,
937 Jashashvili, T., Bruxelles, L., Jakata, K., Bam, L., Van Hoorebeke, L., Kuman, K., Stratford,
938 D., 2020. The atlas of StW 573 and the late emergence of human-like head mobility and
939 brain metabolism. Sci. Rep. 10, 4285.
940 Begun, D.R., 2002. The Pliopithecoidea. In: Hartwig, W.C. (Ed.), The Primate Fossil Record.
941 Cambridge University Press, Cambridge, pp. 221–240.
942 Begun, D.R., 2015. Fossil record of Miocene hominoids. In: Henke, W., Tattersall, I. (Eds.),
943 Handbook of Paleoanthropology, 2nd ed. Springer, Heidelberg, pp. 1261–1332.
944 Begun, D.R., 2017. Evolution of the Pliopithecoidea. In: Fuentes, A. (Ed.), The International
945 Encyclopedia of Primatology. John Wiley & Sons, Hoboken.
946 https://doi.org/10.1002/9781119179313.wbprim0165.
947 Benefit, B.R., 1999. *Victoriapithecus*: the key to Old World monkey and catarrhine origins.
948 Evol. Anthropol. 7, 155–174.

949 Benefit, B.R., McCrossin, M.L., 1997. Earliest known Old World monkey skull. Nature 388,
950 368–371.
951 Benefit, B.R., McCrossin, M.L., 2015. A window into ape evolution. Science 350, 515–516.
952 Bernor, R.L., Flynn, L.J., Harrison, T., Hussain, S.T., Kelley, J., 1988. *Dionysopithecus* from
953 southern Pakistan and the biochronology and biogeography of early Eurasian catarrhines.
954 J. Hum. Evol. 17, 339–358.
955 Blomberg, S.P., Garland, T., Ives, A.R., 2003. Testing for phylogenetic signal in comparative
956 data: behavioral traits are more labile. Evolution, 57, 717–745.
957 Bookstein, F.L., 1991. Morphometric Tools for Landmark Data: Geometry and Biology.
958 Cambridge University Press, Cambridge.
959 Boyer, D.M., Kirk, E.C., Silcox, M.T., Gunnell, G.F., Gilbert, C.C., Yapuncich, G.S., Allen, K.L.,
960 Welch, E., Bloch, J.I., Gonzales, L.A., Kay, R.F., Seiffert, E.R., 2016. Internal carotid arterial
961 canal size and scaling in Euarchonta: Re-assessing implications for arterial patency and
962 phylogenetic relationships in early fossil primates. J. Hum. Evol. 97, 123–144.
963 Boyer, D.M., Harrington, A.R., 2018. Scaling of bony canals for encephalic vessels in
964 euarchontans: Implications for the role of the vertebral artery and brain metabolism. J.
965 Hum. Evol. 114, 85–101.
966 Boyer, D.M., Harrington, A.R., 2019. New estimates of blood flow rates in the vertebral
967 artery of euarchontans and their implications for encephalic blood flow scaling: A
968 response to Seymour and Snelling (2018). J. Hum. Evol. 128, 93–98.
969 Bugge, J., 1974. The cephalic arterial system in insectivores, primates, rodents, and
970 lagomorphs, with special reference to the systematic classification. Acta Anat. 87, 1–160.

971 Bugge, J., 1980. Comparative anatomical study of the carotid circulation in New and Old
972 World Primates. In: Ciochon, R.L., Chiarelli, A.B. (Eds.), Evolutionary Biology of the New
973 World Monkeys and Continental Drift. Plenum Press, New York, pp. 293–316.
974 Cardini, A., O'Higgins, P., Rohlf, F.J., 2019. Seeing distinct groups where there are none:
975 spurious patterns from between-group PCA. Evol. Biol. 46, 303–316.
976 Cardini, A., Polly, P.D., 2020. Cross-validated between group PCA scatterplots: A solution to
977 spurious group separation? Evol. Biol. 47, 85–95.
978 Cartmill, M., MacPhee, R.D.E., Simons, E.L., 1981. Anatomy of the temporal bone in early
979 anthropoids, with remarks on the problem of anthropoid origins. Am. J. Phys. Anthropol.
980 56, 1–21.
981 Casanovas-Vilar, I., Alba, D.M., Garcés, M., Robles, J.M., Moyà-Solà, S., 2011. Updated
982 chronology for the Miocene hominoid radiation in Western Eurasia. Proc. Natl. Acad. Sci.
983 USA 108, 5554–5559.
984 Chatterjee, H.J., Ho, S.Y.W., Barnes, I., Groves, C. 2009. Estimating the phylogeny and
985 divergence times of primates using a supermatrix approach. BMC Evol. Biol. 13, 259.
986 Collyer, M.L., Adams, D.C., 2018. RRPP: An R package for fitting linear models to high-
987 dimensional data using residual randomization. Methods Ecol. Evol. 9, 1772–1779.
988 Delson, E., Terranova, C.J., Sargis, E.J., Jungers, W.L., Jablonski, N.G.C., Dechow, P., 2000.
989 Body mass in Cercopithecidae (Primates, Mammalia): estimation and scaling in extinct
990 and extant taxa. Anthropol. Pap. Am. Mus. Nat. Hist. 83, 1–159.
991 Diogo, R., Wood, B., 2011. Soft-tissue anatomy of the primates: Phylogenetic analyses based
992 on the muscles of the head, neck, pectoral region and upper limb, with notes on the
993 evolution of these muscles. J. Anat. 219, 272–359.

994 Finstermeier, K., Zinner, D., Brameier, M., Meyer, M., Kreuz, E., Hofreiter, M., Roos, C., 2013.
995 A mitogenomic phylogeny of living primates. PLoS One 8, e69504.
996 Gibbs, S., Collard, M., Wood, B., 2000. Soft-tissue characters in higher primate phylogenetics.
997 Proc. Natl. Acad. Sci. USA 97, 11130–11132.
998 Gibbs, S., Collard, M., Wood, B., 2002. Soft-tissue anatomy of the extant hominoids: A review
999 and phylogenetic analysis. J. Anat. 200, 3–49.
1000 Gilbert, C.C., Bibi, F., Hill, A., Beech, M.J., 2014. Early guenon from the late Miocene
1001 Baynunah Formation, Abu Dhabi, with implications for cercopithecoid biogeography and
1002 evolution. Proc. Natl. Acad. Sci. USA 111, 10119–10124.
1003 Gilbert, C.C., Pugh, K.D., Fleagle, J.G., 2020a. Dispersal of Miocene hominoids (and
1004 pliopithecoids) from Africa to Eurasia in light of changing tectonics and climate. In:
1005 Prasad, G.V., Patnaik, R. (Eds.), Biological Consequences of Plate Tectonics. New
1006 Perspectives on post-Gondwana Break-up—A Tribute to Ashok Sahni. Springer, Cham, pp.
1007 393-412.
1008 Gilbert, C.C., Ortiz, A., Pugh, K.D., Campisano, C.J., Patel, B.A., Premjit, N., Fleagle, J.G.,
1009 Patnaik, R., 2020b. New Middle Miocene ape (Primates: Hylobatidae) from Ramnagar,
1010 India fills major gaps in the hominoid fossil record. Proc. R. Soc. B. 287, 20201655.
1011 Gould, S.J., 1966. Allometry and size in ontogeny and phylogeny. Biol. Rev., 41, 587–640.
1012 Harrison, T., 2010. Dendropithecoidea, Proconsuloidea and Hominoidea (Catarrhini,
1013 Primates). In: Werdelin, L., Sanders, W.J. (Eds.), Cenozoic Mammals of Africa. University of
1014 California Press, Berkeley, pp. 429–469.
1015 Harrison, T., 2013. Catarrhine origins. In: Begun, D.R. (Ed.), A Companion to
1016 Paleoanthropology. Blackwell Publishing, Oxford, pp. 376–396.

1017 Harrison, T., 2016. The fossil record and evolutionary history of hylobatids. In: Reichard,
1018 U.H., Hirai, H., Barelli, C. (Eds.), Evolution of Gibbons and Siamang. Phylogeny,
1019 Morphology, and Cognition. Springer, New York, pp. 90–110.
1020 Harrison, T., 2017. Miocene primates. In: Fuentes, A. (Ed.), The International Encyclopedia of
1021 Primatology. John Wiley & Sons, Hoboken.
1022 https://doi.org/10.1002/9781119179313.wbprim0227.
1023 Harrison, T., Gu, Y., 1999. Taxonomy and phylogenetic relationships of early Miocene
1024 catarrhines from Sihong, China. J. Hum. Evol. 37, 225–277.
1025 Harrison, T., Zhang, Y., Wei, G., Sun, C., Wang, Y., Liu, J., Tong, H., Huang, B., Xu, F., 2020. A
1026 new genus of pliopithecoid from the late Early Miocene of China and its implications for
1027 understanding the paleozoogeography of the Pliopithecoidea. J. Hum. Evol. 145, 102838.
1028 Harzhauser, M., Kroh, A., Mandic, O., Piller, W. E., Göhlich, U., Reuter, M., Berning, B., 2007.
1029 Biogeographic responses to geodynamics: A key study all around the Oligo–Miocene
1030 Tethyan Seaway. Zool. Anz. 246, 241–256.
1031 Kay, R.F., Simons, E., Ross, J.L., 2008. The basicranial anatomy of African Eocene/Oligocene
1032 anthropoids. Are there any clues for platyrrhine origins? In: Fleagle, J.G., Gilbert, C.C.
1033 (Eds.), Elwyn Simons: A Search for Origins. Springer, New York, pp. 125–158.
1034 Legendre, P. 2018. lmodel2: Model II Regression. https://cran.r-
1035 project.org/web/packages/lmodel2/index.html.
1036 Lieberman, D.E., 1999. Homology and hominid phylogeny: Problems and potential solutions.
1037 Evol. Anthropol. 7, 142–151.
1038 Lieberman, D.E., McCarthy, R.C., 1999. The ontogeny of cranial base angulation in humans
1039 and chimpanzees and its implications for reconstructing pharyngeal dimensions. J. Hum.
1040 Evol. 36, 487–517.

1041 Lieberman, D.E., Ross, C.F., Ravosa, M.J., 2000. The primate cranial base: Ontogeny,
1042 function, and integration. Yearbk. Phys. Anthropol. 43, 117–169.
1043 MacPhee, R.D.E., Cartmill, M., 1986. Basicranial structures and primate systematics. In:
1044 Swisher, D.R., Erwin, J. (Eds.), Comparative Primate Biology: Systematics, Evolution, and
1045 Anatomy. Alan R. Liss, New York, pp. 219–275.
1046 McNulty, K.P., Begun, D.R., Kelley, J., Manthi, F.K., Mbua, E.N., 2015. A systematic revision of
1047 *Proconsul* with the description of a new genus of early Miocene hominoid. J. Hum. Evol.
1048 84, 42–61.
1049 Meyer, D., Rinaldi, Ir.D., Ramlee, H., Perwitasari-Farajallah, D., Hodges, J.K., Roos, C., 2011.
1050 Mitochondrial phylogeny of leaf monkeys (genus *Presbytis*, Eschscholtz, 1821) with
1051 implications for taxonomy and conservation. Mol. Phylogenet. Evol. 59, 311–319.
1052 Nengo, I., Tafforeau, P., Gilbert, C.C., Fleagle, J.G., Miller, E.R., Feibel, C., Fox, D.L., Feinberg,
1053 J., Pugh, K.D., Berruyer, C., Mana, S., Engle, Z., Spoor, F., 2017. New infant cranium from
1054 the African Miocene sheds light on ape evolution. Nature 548, 169–174.
1055 Pagel, M., 1999. Inferring the historical patterns of biological evolution. Nature 401, 877–
1056 884.
1057 Perelman, P., Johnson, W.E., Roos, C., Seuánez, H.N., Horvath, J.E., Moreira, M.A.M., Kessing,
1058 B., Pontius, J., Roelke, M., Rumpler, Y., Schneider, M.P.C., Silva, A., O'Brien, S.J., Pecon-
1059 Slattery, J., 2011. A molecular phylogeny of living primates. PLoS Genetics 7, e1001342.
1060 Pozzi, L., Hodgson, J.A., Burrell, A.S., Sterner, K.N., Raaum, R.L., Disotell, T.R., 2014. Primate
1061 phylogenetic relationships and divergence dates inferred from complete mitochondrial
1062 genomes. Mol. Phylogenet. Evol. 75, 165–183.
1063 R Core Team, 2020. R: A language and environment for statistical computing. R Foundation
1064 for Statistical Computing, Vienna.

1065 Rae, T.C., 1999. Mosaic evolution in the origin of the Hominoidea. Folia Primatol. 70, 125–
1066 135.
1067 Revell, L.J., 2012. *Phytools*: an R package for phylogenetic comparative biology (and other
1068 things). Methods Ecol. Evol. 3, 217–223.
1069 Roos, C., Kothe, M., Alba, D.M., Delson, E., Zinner, D., 2019. The radiation of macaques out
1070 of Africa: Evidence from mitogenome divergence times and the fossil record. J. Hum. Evol.
1071 133, 114–132.
1072 Rosenberger, A.L., Szalay, F., 1980. On the tarsiiform origins of the Anthropoidea. In:
1073 Ciochon, R.L., Chiarelli, A.B. (Eds.), Evolutionary Biology of the New World Monkeys and
1074 Contnental Drift. Plenum Press, New York, pp. 139–157.
1075 Ross, C., 1994. Evidence for anthropoid and tarsier relationships. In: Fleagle, J.G., Kay, R.F.
1076 (Eds.), Anthropoid Origins. Plenum Press, New York, pp. 469–547.
1077 Ross, C., Williams, B., Kay, R.F., 1998. Phylogenetic analysis of anthropoid relationships. J.
1078 Hum. Evol. 35, 221–307.
1079 Rossie, J.B., Hill, A., 2018. A new species of *Simiolus* from the middle Miocene of the Tugen
1080 Hills, Kenya. J. Hum. Evol. 125, 50–58.
1081 Sankhyan, A.R., Kelley, J., Harrison, T., 2017. A highly derived pliopithecoid from the Late
1082 Miocene of Haritalyangar, India. J. Hum. Evol 105, 1–12.
1083 Schlager, S., 2017. Morpho and Rvcg e shape analysis in R: R-packages for geometric
1084 morphometrics, shape analysis and surface manipulations. In: Zheng, G., Li, S., Székely, G.
1085 (Eds.), Statistical Shape and Deformation Analysis. Methods, Implementation and
1086 Applications. Academic Press, London, pp. 217–256. https://cran.r-
1087 project.org/web/packages/Morpho/index.html.
1088 Schliep, K.P., 2011. phangorn: phylogenetic analysis in R. Bioinformatics 27, 592–593.

1089 Seiffert, E.R., 2006. Revised age estimates for the later Paleogene mammal faunas of Egypt
1090 and Oman. Proc. Natl. Acad. Sci. USA 103, 5000–5005.
1091 Seiffert, E.R., 2012. Early primate evolution in Afro-Arabia. Evol. Anthropol. 21, 239–253.
1092 Seiffert, E.R., Simons, E.L., Fleagle, J.G., Godinot, M., 2010. Paleogene anthropoids. In:
1093 Werdelin, L., Sanders, W.J. (Eds.), Cenozoic Mammals of Africa. University of California
1094 Press, Berkeley, pp. 369–391.
1095 Shoshani, J., Groves, C.P., Simons, E.L., Gunnell, G.F., 1996. Primate phylogeny:
1096 Morphological vs molecular results. Mol. Phylogenet. Evol. 5, 102–154.
1097 Sidlauskas, B., 2008. Continuous and arrested morphological diversification in sister clades of
1098 characiform fishes: aphylomorphospace approach. Evolution 62, 3135–3156.
1099 Smith, R.J., Jungers, W.L., 1997. Body mass in comparative primatology. J. Hum. Evol. 32,
1100 523–559.
1101 Springer, M.S., Meredith, R.W., Gatesy, J., Emerling, C.A., Park, J., Rabosky, D.L., Stadler, T.,
1102 Steiner, C., Ryder, O.A., Janečka, J.E., Fisher, C.A., Murphy, W.J., 2012. Macroevolutionary
1103 dynamics and historical biogeography of primate diversification inferred from a species
1104 supermatrix. PLoS One 7, e49521.
1105 Stevens, N.J., Seiffert, E.R., O'Connor, P.M., Roberts, E.M., Schmitz, M.D., Krause, C.,
1106 Gorscak, E., Ngasala, S., Hieronymus, T.L., Temu, J., 2013. Palaeontological evidence for
1107 an Oligocene divergence between Old World monkeys and apes. Nature 497, 611–614.
1108 Turner, T.R., Schmitt, C.A., Cramer, J.D., Lorenz, J., Grobler, J.P., Jolly, C.J., Freimer, N.B.,
1109 2018. Morphological variation in the genus *Chlorocebus*: Ecogeographic and
1110 anthropogenically mediated variation in body mass, postcranial morphology, and growth.
1111 Am. J. Phys. Anthropol. 166 (S3), 682–707.

Urciuoli, A., Zanolli, C., Beaudet, A., Dumoncel, J., Santos, F., Moyà-Solà, S., Alba, D.M., 2020. The evolution of the vestibular apparatus in apes and humans. eLife 9, e51261.

Urciuoli, A., Zanolli, C., Beaudet, A., Pina, M., Almécija, S., Moyà-Solà, S., Alba, D.M., 2021a. A comparative analysis of the vestibular apparatus in *Epipliopithecus vindobonensis*: Phylogenetic implications. J. Hum. Evol. 151, 102930.

Urciuoli, A., Zanolli, C., Almécija, S., Beaudet, A., Dumoncel, J., Morimoto, N., Nakatsukasa, M., Moyà-Solà, S., Begun, D.R., Alba, D.M., 2021b. Reassessment of the phylogenetic relationships of the late Miocene apes *Hispanopithecus* and *Rudapithecus* based on vestibular morphology. Proc. Natl. Acad. Sci. USA 118, e2015215118.

Walker, A., Teaford, M.F., Martin, L., Andrews, P., 1993. A new species of *Proconsul* from the early Miocene of Rusinga/Mfangano Islands, Kenya. J. Hum. Evol. 25, 43–53.

Zalmout, I.S., Sanders, W.J., MacLatchy, L., Gunnell, G., Al-Mufarreh, Y.A., Ali, M.A., Nasser, A.-A.H., Al-Masary, A.M., Al-Sobhi, S.A., Nadhra, A.O., Matari, A.H., Wilson, J.A., Gingerich, P.D., 2010. New Oligocene primate from Saudi Arabia and the divergence of apes and Old World monkeys. Nature 466, 360–365.

Zapfe, H., 1961. Die Primatenfunde aus der miozänen Spaltenfüllung von Neudorf an der March (Děvínská Nová Ves), Tschechoslowakei. Schweizer. Palaeontol. Abh. 78, 1–293.

Figure captions

Figure 1. Schematic illustration of the protocol used in this study for cutting the extremities of the carotid canal as exemplified in a *Macaca fascicularis* individual. a) To cut the posterior end, a best-fit plane defined for the landmarks placed at the carotid foramen is computed. b) To cut the anterior end, the 3D canal surface is first imported as a cloud of points in R. c) The

projection of IRG on the cloud of points (IRG') is computed. d) 360 points are created around the axis IRG–IRG'. e, f) 360 possible cutting planes passing through IRG are created (each being based on IRG, IRG' and one of the points rotating around the axis), here depicted in anterior (e) and superior (f) views. The cross-sectional area obtained by cutting the canal using each possible plane is calculated as follows: g–i) the points of the cloud belonging to the plane are recorded (g), the most external points (in red) are kept to create a convex hull that approximates the shape of the canal contour (h), and a set of triangles is drawn, each of them having the same point of the contour as the most acute vertex, and the two subsequent points on the contour as the other vertices (i); the total area is the obtained by summing those of each individual triangle. j, k) The plane with the smallest cross-sectional area (that is, orthogonal to the 3D canal surface and therefore to the canal streamline) (j) is used as a reference for cutting the canal at its anterior end (k). l) The centroids of the (posterior) carotid foramen landmark set and of the anterior cross-section (i.e., obtained by cutting with the orthogonal plane), representing the posterior and anterior endpoints of the carotid canal, respectively, are calculated. IRG = Intersection ridge–groove; IRG' = orthogonal projection on the 3D carotid canal surface of IRG.

Figure 2. Petrosal landmarks used for aligning the specimens as exemplified in a *Macaca fascicularis* individual in different views: a) right lateral; b) inferior; c) sagittal cross section (right-mirrored for visualization purpose); d) superior transverse cross section. Landmarks: 1 = porion; 2 = inferior external auditory meatus; 3 = posterior external auditory meatus; 4 = posterior internal auditory meatus; 5 = anterior internal auditory meatus; 6 = medial anterior pyramidal ridge; 7 = intersection ridge-groove; 8 = greater superficial petrosal nerve hiatus; 9 = stylomastoid foramen.

Figure 3. Graphic representation of the 2D angles defining the carotid canal orientation relative to the cranium. a) Virtual external reconstructions of the cranium, in superior (left) and lateral (right) views. b) Virtual cross sections of the cranium to visualize the petrosal bone, in transverse (left) and sagittal (right) views. c) Representations of the carotid canal medial orientation (2DXYA; left) and superior orientation (2DYZA; right) within the cranium, rendered in semitransparency; red lines represent the 2D canal vector and its direction, orange squares represent the plane along which the angle can vary, and dotted black lines represent the standard reference vector. For 2DXYA, the plane of angle variation is a transverse plane, whereas for 2DYZA the plane of angle variation is a (para)sagittal plane. For both angles, the standard reference vector is a 2D vector parallel to the anteroposterior cranial axis (from posterior to anterior). Both angles are calculated between the 2D canal vector and the 2D standard reference vector. Because the anthropoid mean configuration is extremely similar to the canal course configuration of *Presbytis* (i.e., before alignment), the cranium of this taxon is used as a reference for orienting the canal following the cranial axes of reference.

Figure 4. Virtual reconstructions of carotid canal comparing *Pliobates* with extant anthropoids and some Miocene catarrhines: a) *Pliobates* (IPS58443.1); b) *Epipliopithecus* (NHMW 1970/1397/0003); c) *Ekembo* (KNM-RU 2036al); d) *Victoriapithecus* (KNM-MB 29100); e) *Alouatta*; f) *Aotus*; g) *Cebus*; h) *Mico*; i) *Plecturocebus*; j) *Cercopithecus*; k) *Colobus*; l) *Mandrillus*; m) *Presbytis*; n) *Hylobates*; o) *Hoolock*; p) *Nomascus*; q) *Symphalangus*; r) *Gorilla*; s) *Pan*; t) *Pongo*. The canals are shown in medial view with their posterior ends horizontally aligned. Scale bars = 5 mm.

Figure 5. Box-and-whisker plots of the variables describing the orientation, proportions and course of the carotid canal in the fossil specimens and main extant clades analyzed in this study: a) 2D YZ angle; b) 2D XY angle; c) index $L/V^{(1/3)}$; d) bgPC1; e) bgPC2. Horizontal lines denote medians, boxes depict the interquartile range, whiskers the minimum-maximum values excluding outliers, dots denote outliers (beyond 1.5 times above or below the interquartile range). Abbreviations: L = length (in mm); V = volume (in mm^3); bgPC = between-group principal component; 2DYZA = 2D angle in the YZ plane (canal superior orientation; in degrees); 2DXYA = 2D angle in the XY plane (canal medial orientation; in degrees).

Figure 6. Results of the between-group principal component analysis (bgPCA) based on carotid canal course variation among main extant anthropoid clades. a) Bivariate plot of bgPC2 vs. bgPC1 (the variance explained by each bgPC is denoted in parentheses). b) Minimum (blue) and maximum (red) landmark conformations compared with the anthropoid mean configuration (black) for bgPC1 and bgPC2, in superior (top), lateral (middle), and anterior (bottom) views (anatomical axes of reference are specified next to each view; see Fig. 7 for a representation of the carotid canal within the cranium). Convex hulls correspond to: platyrrhines (blue), cercopithecids (red), hylobatids (green), and hominids (gray). Abbreviation: bgPC = between-group principal component.

Figure 7. Representations of the carotid canal relative to the cranium in superior (left), lateral (middle), and anterior (right) views. a) Virtual external reconstruction of the cranium. b) Virtual cross sections of the cranium to visualize the petrosal bone (from left to right,

transverse, sagittal, and coronal sections are depicted). c) Virtual reconstructions of the carotid canal within the cranium rendered in semitransparency. d, e) Minimum (blue) and maximum (red) landmark conformations compared with the anthropoid mean configuration (black) for bgPC1 (d) and bgPC2 (e) within the cranium rendered in semitransparency. Because the anthropoid mean configuration is extremely similar to the canal course configuration of *Presbytis* (i.e., before alignment), the cranium of this taxon is used as a reference for orienting the canal following the cranial axes of reference.

Figure 8. Neighbor-joining cluster (unrooted) based on the Euclidean distances calculated from raw coordinates of the canal course configurations in *Pliobates*, extant anthropoids and other Miocene catarrhines. Cophenetic = 0.94.

Figure 9. Phylomorphospace of carotid canal course variation in extant anthropoids and extinct Miocene catarrhines including *Pliobates*. *Epipliopithecus* and *Pliobates* are considered sister taxa within a stem catarrhine pliopithecoid clade and *Ekembo* is considered a stem hominoid while *Victoriapithecus* is considered a stem cercopithecoid (see SOM Fig. S2b for a representation of this phylogenetic hypothesis). Ancestral nodes: 1 = crown platyrrhines; 2 = crown catarrhines; 3 = crown cercopithecoids; 4 = crown hominoids; 5 = crown hominids; 6 = crown hylobatids. See SOM Figure S8 for a phylomorphospace derived from the alternative phylogenetic hypothesis (SOM Fig. S2b).

Figure 10. Configurations of the carotid canal course in *Pliobates* compared with other Miocene catarrhines and the reconstructed carotid canal course for the last common ancestors (LCAs) of various anthropoid clades: a) *Pliobates* (IPS58443.1); b) *Epipliopithecus*

(NHMW 1970/1397/0003); c) *Ekembo* (KNM-RU 2036al); d) *Victoriapithecus* (KNM-MB 29100); e) crown platyrrhines; f) crown catarrhines; g) crown cercopithecoids; h) crown hominoids; i) crown hylobatids; j) crown hominids. The canal courses of the LCAs have been inferred based on the phylomorphospace displayed in Figure 9 (see SOM Fig. S9 for the inferred LCA configurations derived from the alternative phylogenetic hypothesis). For each specimen/LCA, the configurations are displayed in superior (left), lateral (middle), and anterior (right) views. The mean configuration computed for the whole anthropoid sample is represented by black dots, while configurations for Miocene catarrhines and LCAs are represented in beige. The anthropoid mean configuration was used as a reference for visualizing all the configurations at the same relative scale.

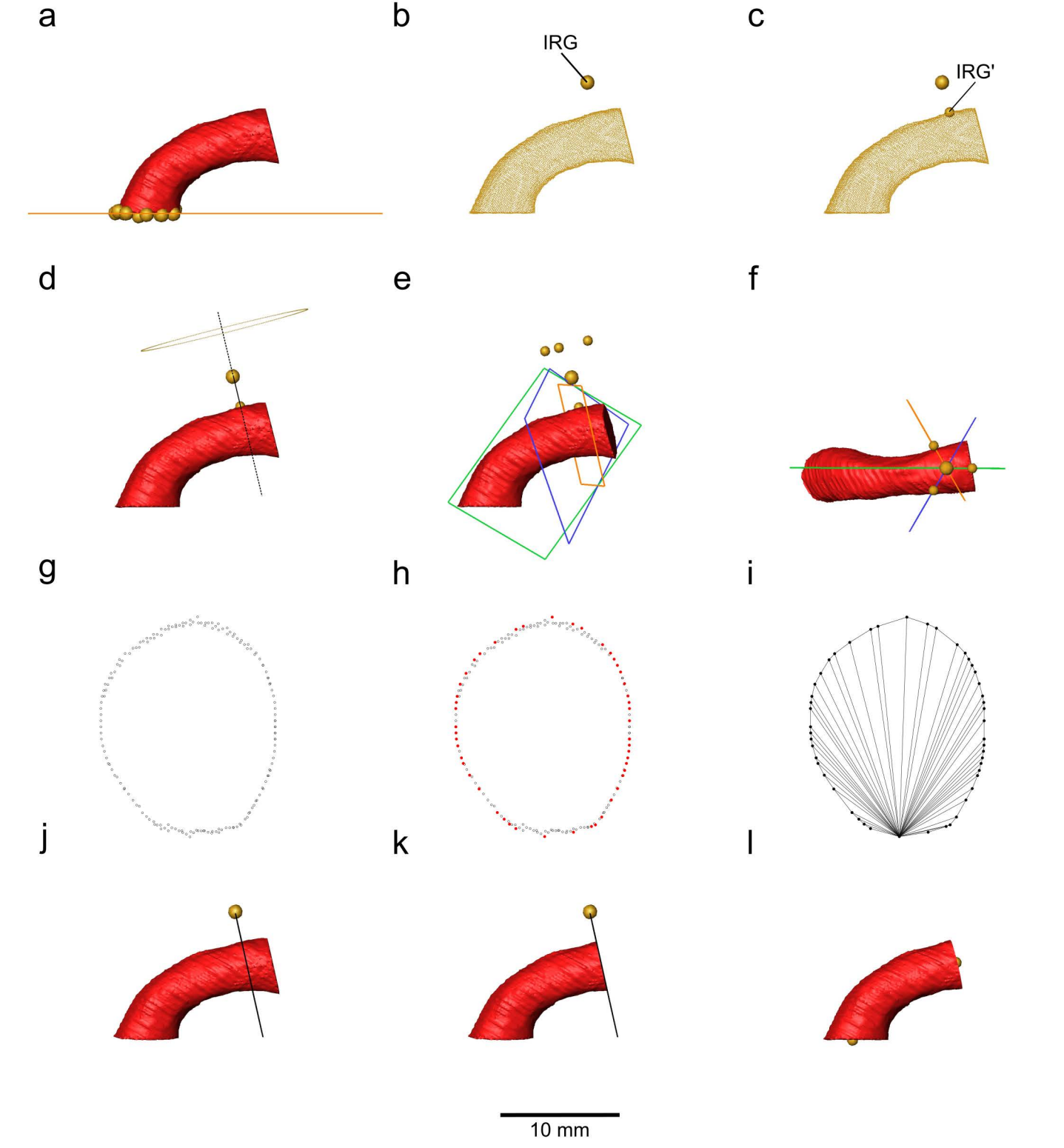
a
b
IRG
c
IRG'
d
e
f
g
h
i
j
k
l
10 mm

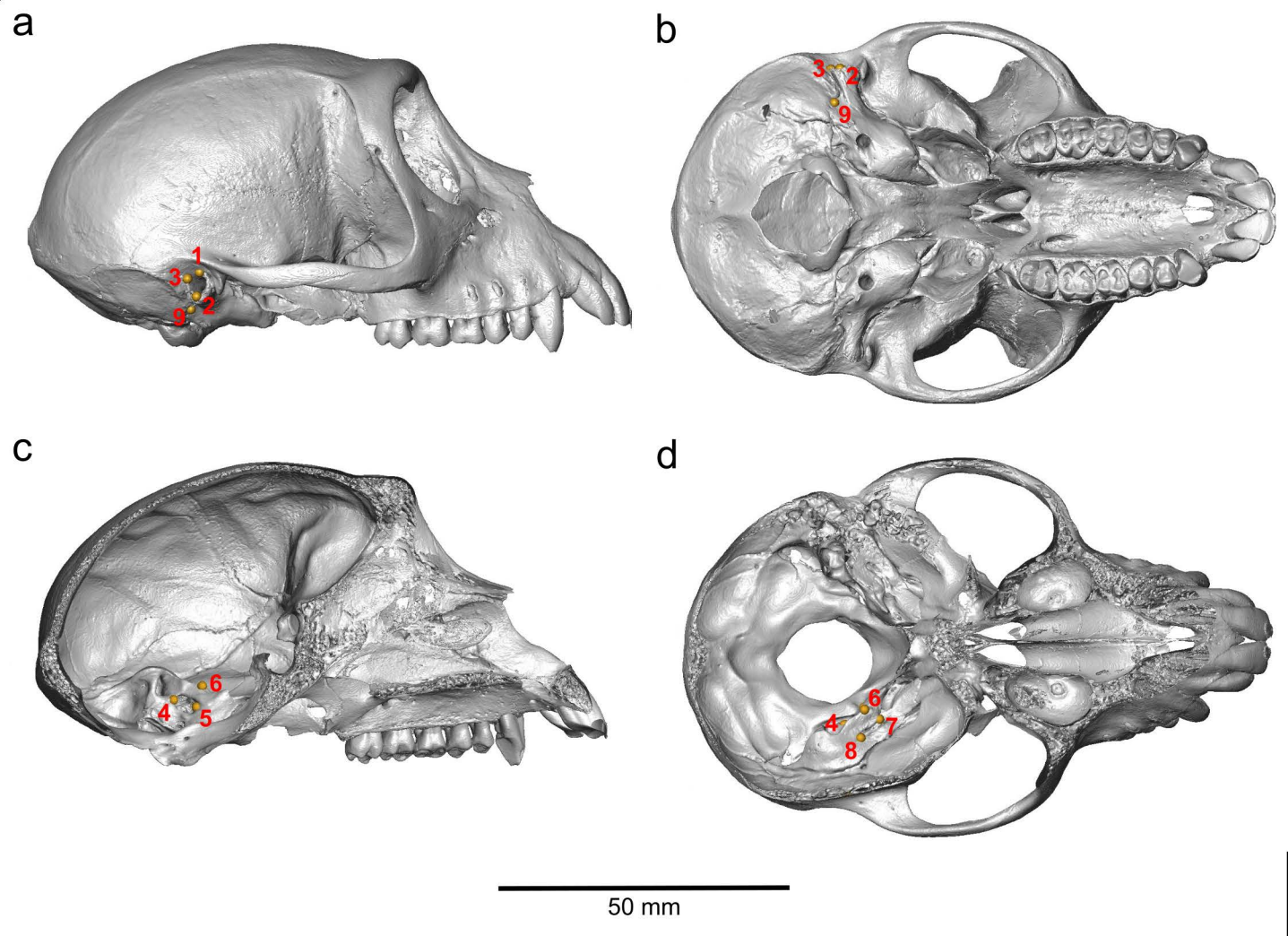
a
1
3
2
9
b
3
2
9
c
6
4
5
d
6
4
7
8
50 mm

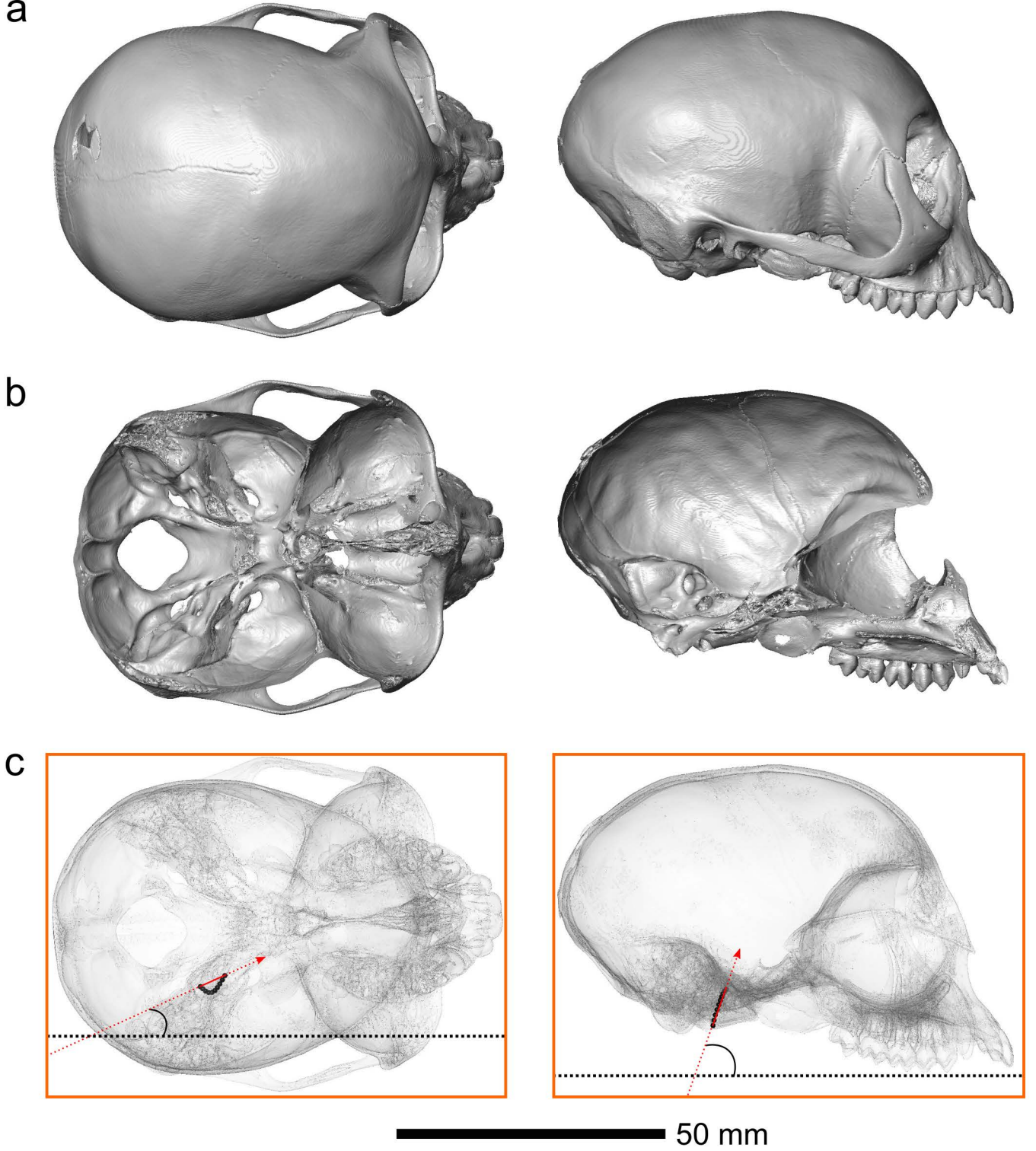
a
b
c
50 mm

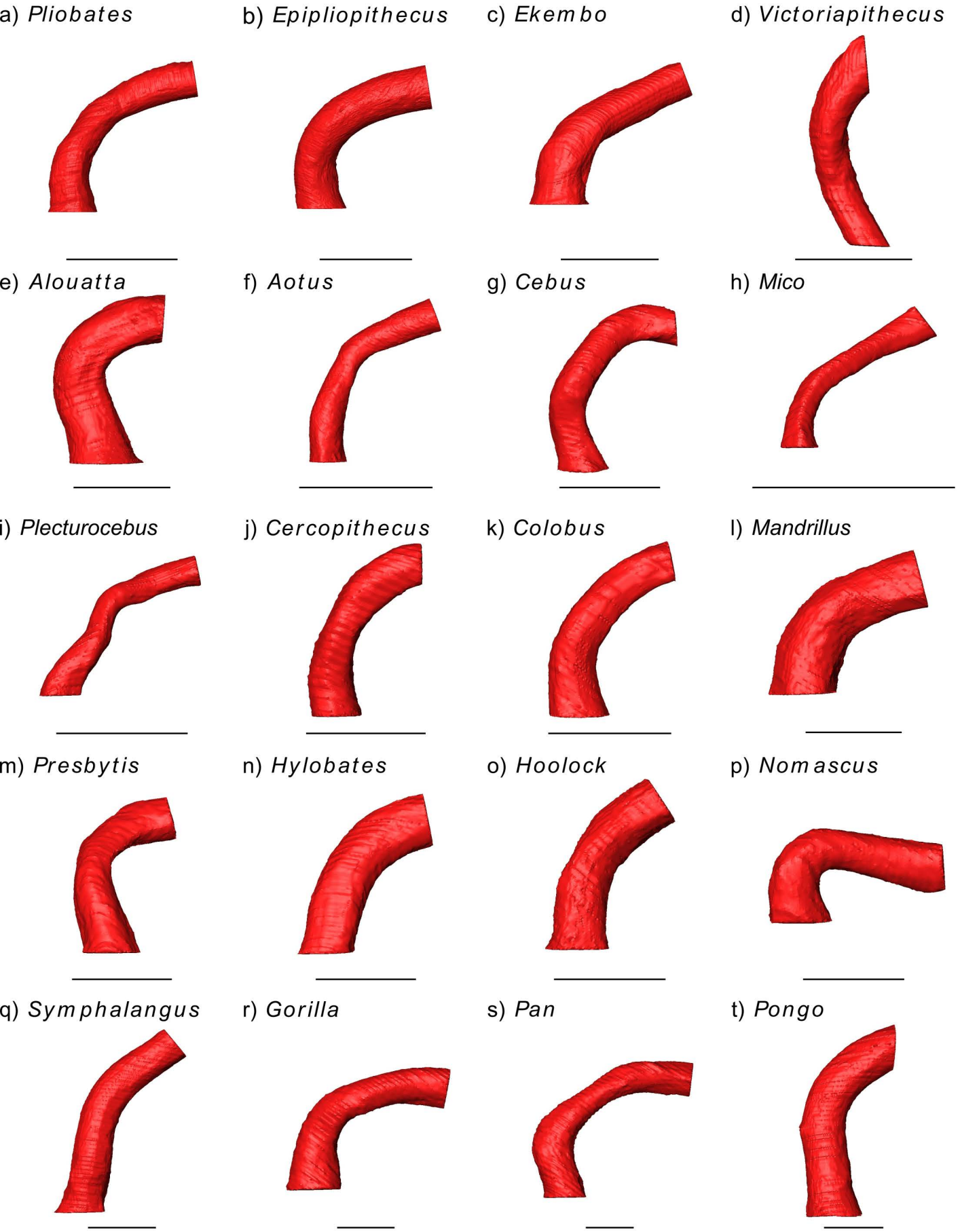
a) Pliobates
b) Epipliopithecus
c) Ekembo
d) Victoriapithecus
e) Alouatta
f) Aotus
g) Cebus
h) Mico
i) Plecturocebus
j) Cercopithecus
k) Colobus
l) Mandrillus
m) Presbytis
n) Hylobates
o) Hoolock
p) Nomascus
q) Symphalangus
r) Gorilla
s) Pan
t) Pongo

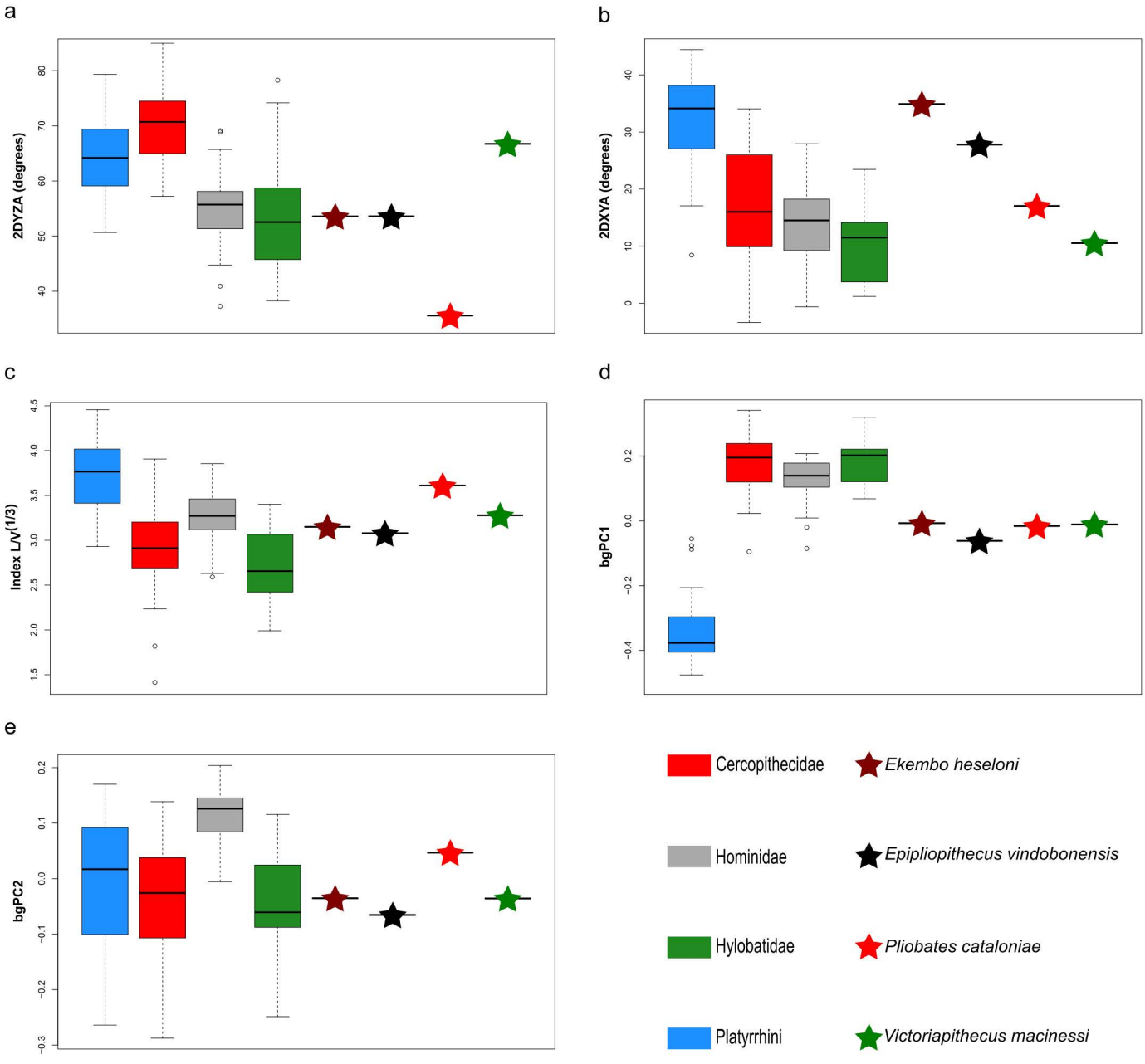
a
2DYZA (degrees)
b
2DXYA (degrees)
c
Index L/V(1/3)
d
bgPC1
e
bgPC2
Cercopithecidae
Hominidae
Hylobatidae
Platyrrhini
Ekembo heseloni
Epipliopithecus vindobonensis
Pliobates cataloniae
Victoriapithecus macinessi

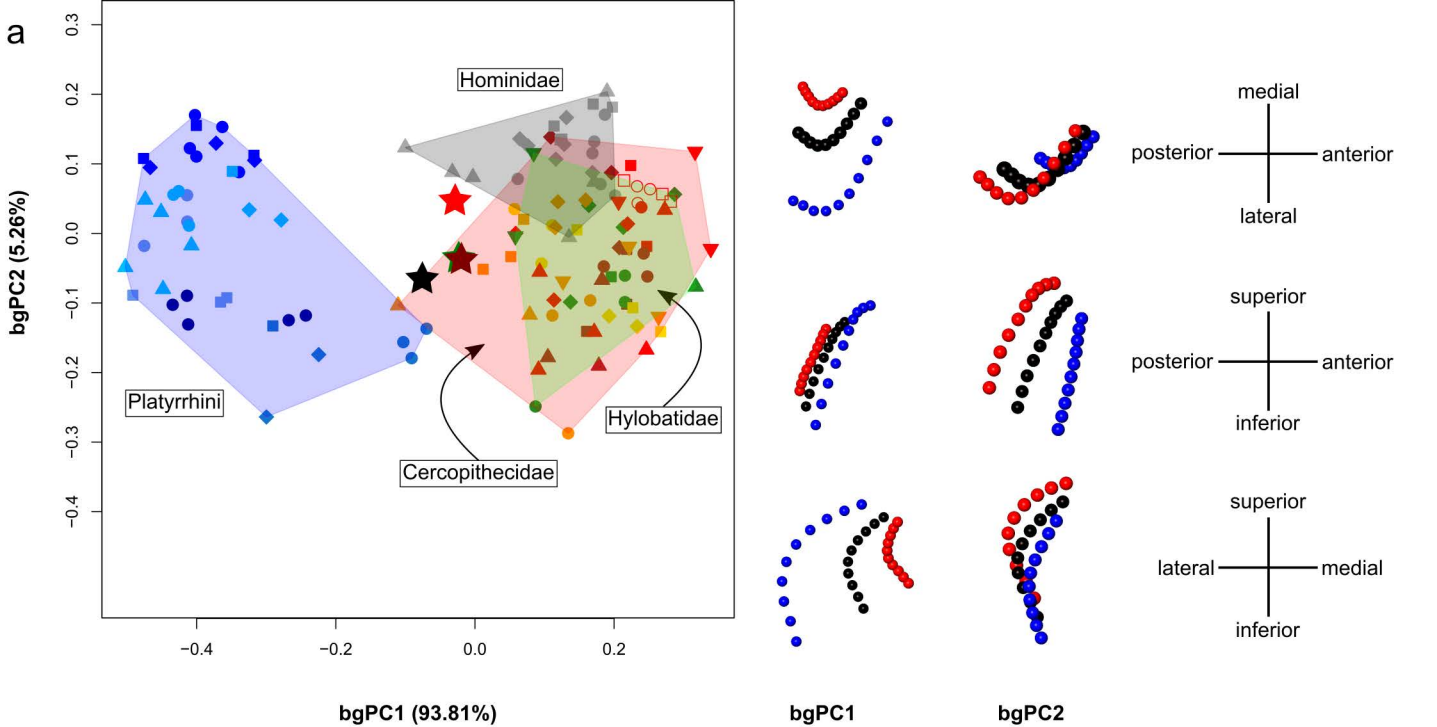

- *Alouatta palliata*
- *Ateles geoffroyi*
- *Lagothrix lagotricha*
- *Aotus griseimembra*
- *Mico argentatus*
- *Saguinus fuscicollis*
- *Saguinus midas*
- *Cebus imitator*
- *Saimiri sciureus*
- *Chiropotes chiropotes*
- *Pithecia monachus*
- *Pithecia pithecia*
- *Plecturocebus cupreus*
- *Cercocebus galeritus*
- *Cercocebus torquatus*
- *Lophocebus albigena*
- *Macaca fascicularis*
- *Mandrillus sphinx*
- *Papio anubis*
- *Theropithecus gelada*
- *Cercopithecus mitis*
- *Chlorocebus pygerythrus*
- *Erythrocebus patas*
- *Miopithecus talapoin*
- *Colobus guereza*
- *Piliocolobus badius*
- *Procolobus verus*
- *Nasalis larvatus*
- *Presbytis rubicunda*
- *Semnopithecus entellus*
- *Simias concolor*
- *Trachypithecus cristatus*
- *Gorilla gorilla*
- *Pan paniscus*
- *Pan troglodytes*
- *Pongo* sp.
- *Hoolock hoolock*
- *Hylobates agilis*
- *Hylobates lar*
- *Nomascus leucogenys*
- *Symphalangus syndactylus*
- *Ekembo heseloni*
- *Epipliopithecus vindobonensis*
- *Pliobates cataloniae*
- *Victoriapithecus macinessi*

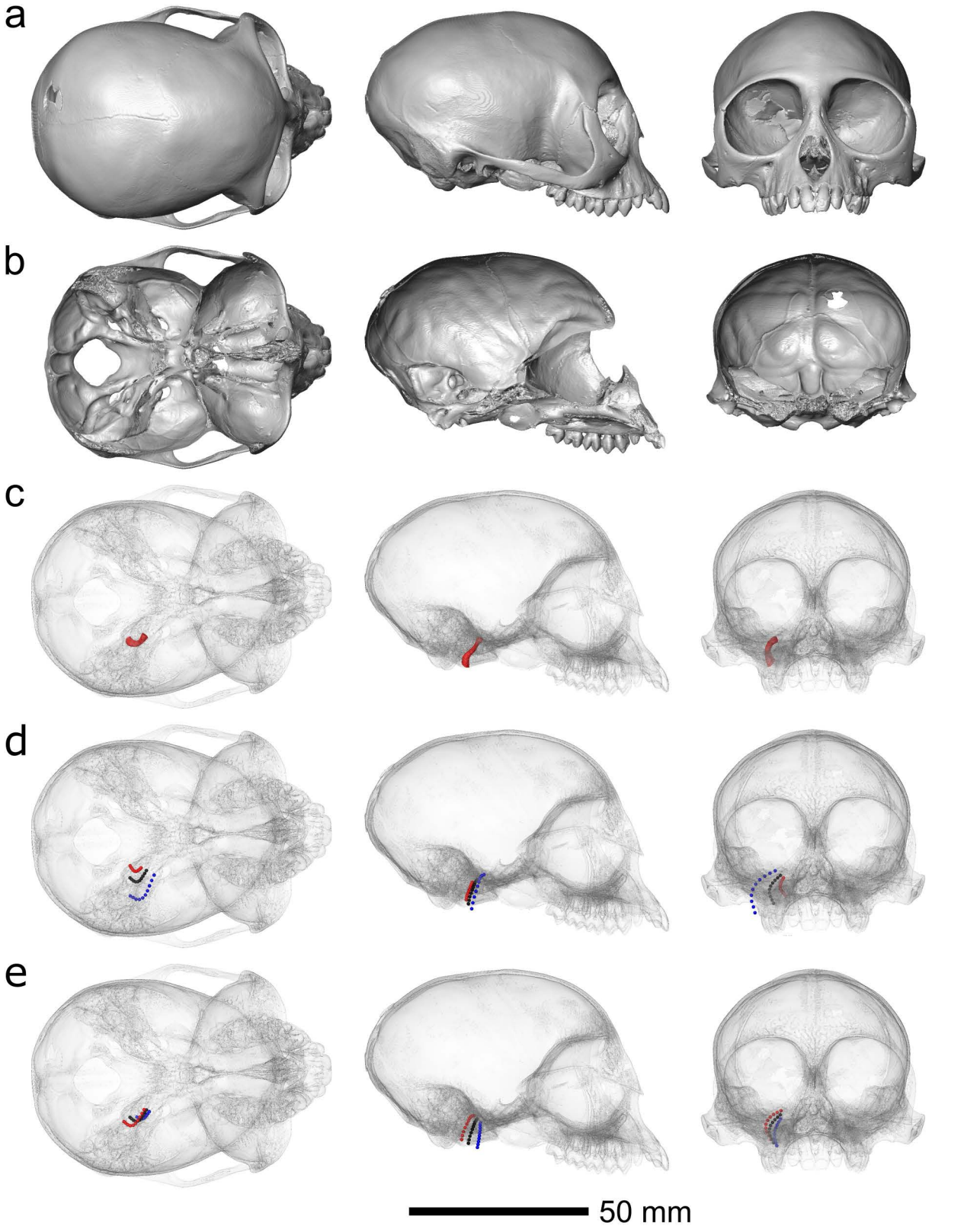
a
b
c
d
e
50 mm

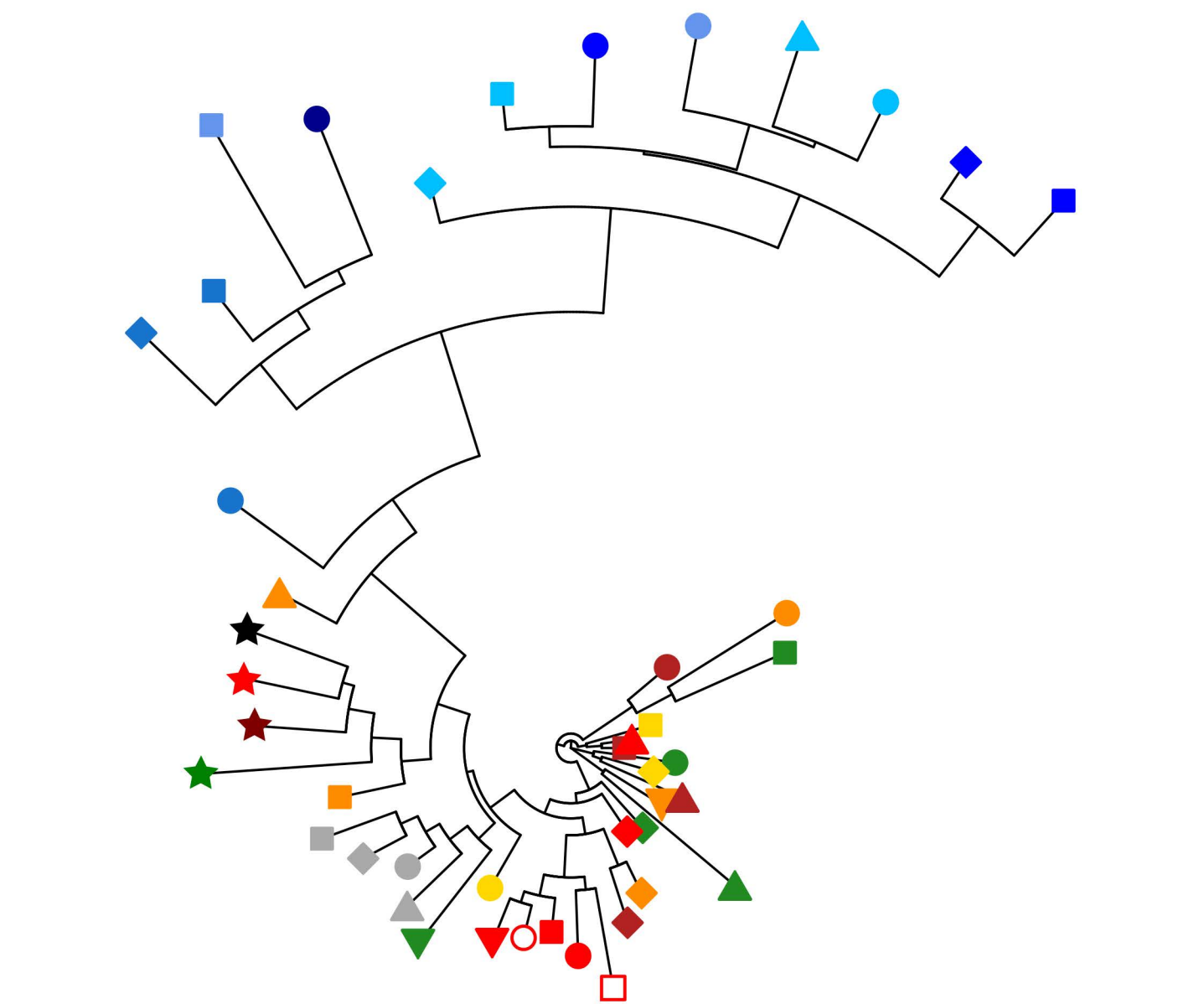

- *Alouatta palliata*
- *Ateles geoffroyi*
- *Lagothrix lagotricha*
- *Aotus griseimembra*
- *Mico argentatus*
- *Saguinus fuscicollis*
- *Saguinus midas*
- *Cebus imitator*
- *Saimiri sciureus*
- *Chiropotes chiropotes*
- *Pithecia monachus*
- *Pithecia pithecia*
- *Plecturocebus cupreus*
- *Cercocebus galeritus*
- *Cercocebus torquatus*
- *Lophocebus albigena*
- *Macaca fascicularis*
- *Mandrillus sphinx*
- *Papio anubis*
- *Theropithecus gelada*
- *Cercopithecus mitis*
- *Chlorocebus pygerythrus*
- *Erythrocebus patas*
- *Miopithecus talapoin*
- *Colobus guereza*
- *Piliocolobus badius*
- *Procolobus verus*
- *Nasalis larvatus*
- *Presbytis rubicunda*
- *Semnopithecus entellus*
- *Simias concolor*
- *Trachypithecus cristatus*
- *Gorilla gorilla*
- *Pan paniscus*
- *Pan troglodytes*
- *Pongo* sp.
- *Hoolock hoolock*
- *Hylobates agilis*
- *Hylobates lar*
- *Nomascus leucogenys*
- *Symphalangus syndactylus*
- *Ekembo heseloni*
- *Epipliopithecus vindobonensis*
- *Pliobates cataloniae*
- *Victoriapithecus macinessi*

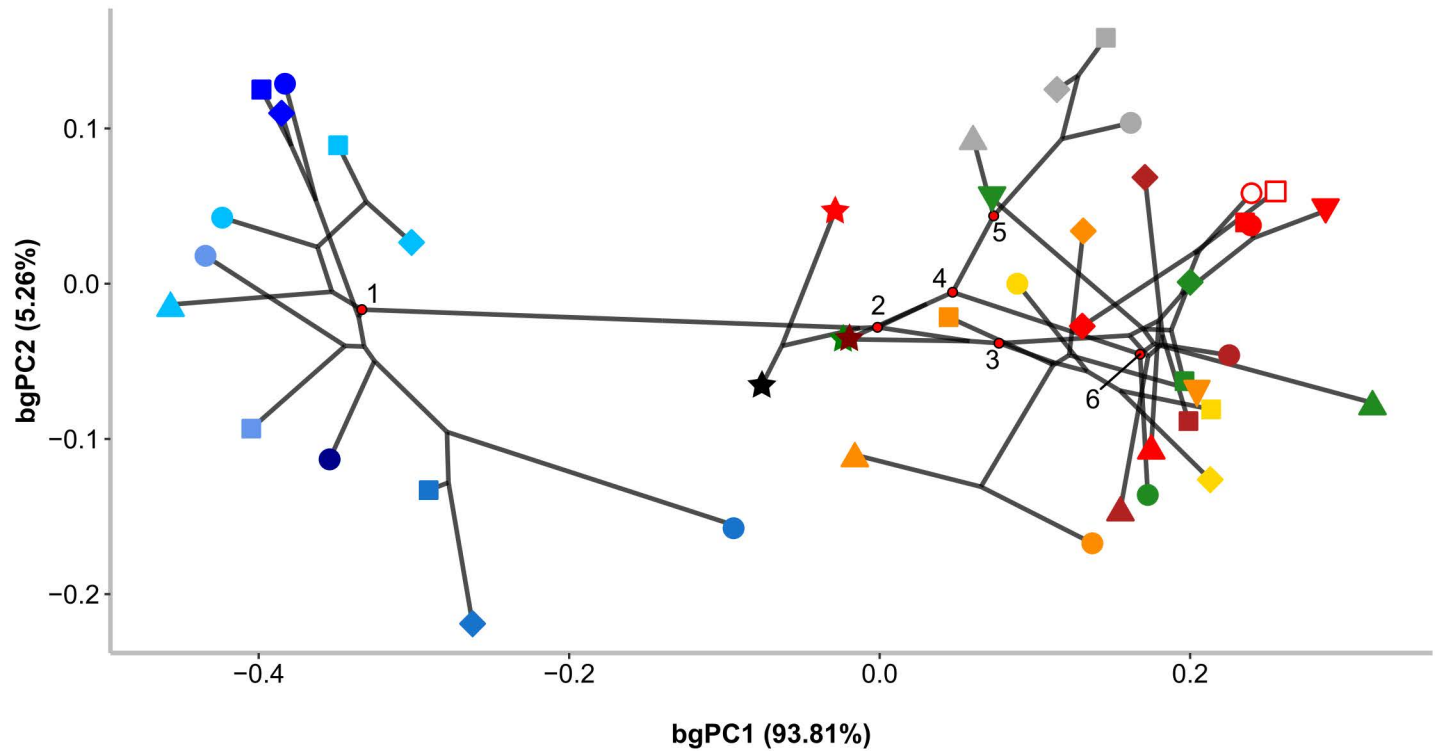

- *Alouatta palliata*
- *Ateles geoffroyi*
- *Lagothrix lagotricha*
- *Aotus griseimembra*
- *Mico argentatus*
- *Saguinus fuscicollis*
- *Saguinus midas*
- *Cebus imitator*
- *Saimiri sciureus*
- *Chiropotes chiropotes*
- *Pithecia monachus*
- *Pithecia pithecia*
- *Plecturocebus cupreus*
- *Cercocebus galeritus*
- *Cercocebus torquatus*
- *Lophocebus albigena*
- *Macaca fascicularis*
- *Mandrillus sphinx*
- *Papio anubis*
- *Theropithecus gelada*
- *Cercopithecus mitis*
- *Chlorocebus pygerythrus*
- *Erythrocebus patas*
- *Miopithecus talapoin*
- *Colobus guereza*
- *Piliocolobus badius*
- *Procolobus verus*
- *Nasalis larvatus*
- *Presbytis rubicunda*
- *Semnopithecus entellus*
- *Simias concolor*
- *Trachypithecus cristatus*
- *Gorilla gorilla*
- *Pan paniscus*
- *Pan troglodytes*
- *Pongo* sp.
- *Hoolock hoolock*
- *Hylobates agilis*
- *Hylobates lar*
- *Nomascus leucogenys*
- *Symphalangus syndactylus*
- *Ekembo heseloni*
- *Epipliopithecus vindobonensis*
- *Pliobates cataloniae*
- *Victoriapithecus macinessi*

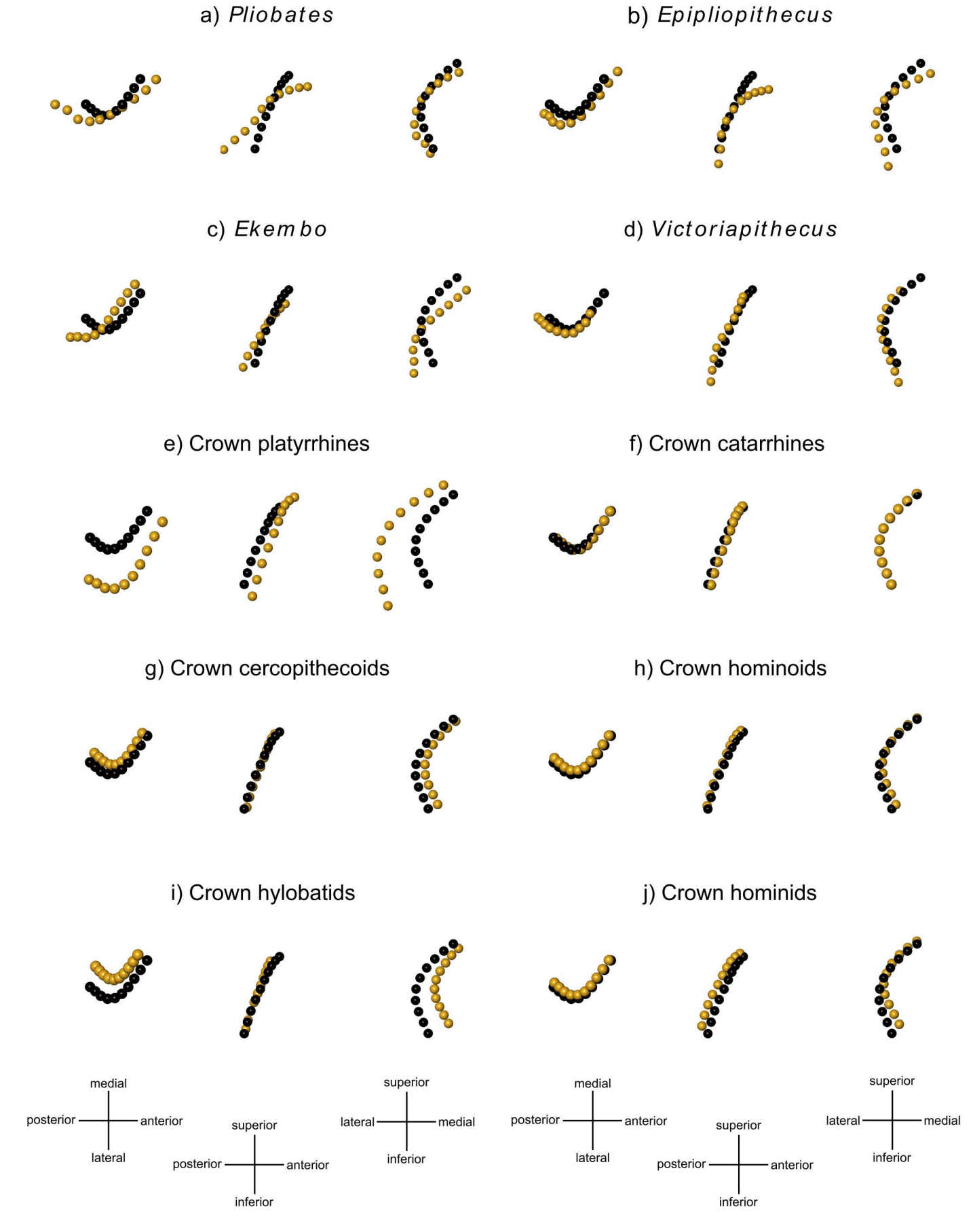
a) *Pliobates*
b) *Epipliopithecus*
c) *Ekembo*
d) *Victoriapithecus*
e) Crown platyrrhines
f) Crown catarrhines
g) Crown cercopithecoids
h) Crown hominoids
i) Crown hylobatids
j) Crown hominids
medial
posterior
anterior
lateral
superior
posterior
anterior
inferior
superior
lateral
medial
inferior
medial
posterior
anterior
lateral
superior
posterior
anterior
inferior
superior
lateral
medial
inferior

Table 1

Extant comparative sample used in this study based on µCT scans. Sample size and sex composition, institutional repository for the specimens, digital repository source, and voxel size range are indicated for each species. See SOM Table S1 for further details on the specimens included.

Taxon	Species	*n*	M	F	?	Repository	Source	Voxel size (µm)
Platyrrhini	*Alouatta palliata*	5	2	3	0	DUEA	MS	52–67
Platyrrhini	*Aotus griseimembra*	5	2	3	0	USNM	MS	34–38
Platyrrhini	*Ateles geoffroyi*	3	0	3	0	AMNH, MCZ	MS	62–63
Platyrrhini	*Cebus imitator*	3	0	3	0	MCZ	MS	80
Platyrrhini	*Chiropotes chiropotes*	3	1	2	0	USNM	MS	47–49
Platyrrhini	*Lagothrix lagotricha*	3	1	2	0	USNM	MS	58–60
Platyrrhini	*Mico argentatus*	3	2	1	0	MCZ	MS	40
Platyrrhini	*Pithecia monachus*	1	0	0	1	MCZ	MS	50
Platyrrhini	*Pithecia pithecia*	2	1	1	0	MCZ	MS	50
Platyrrhini	*Plecturocebus cupreus*	5	3	2	0	AMNH, MCZ	MS	47–51
Platyrrhini	*Saguinus fuscicollis*	1	0	1	0	AMNH	MS	27
Platyrrhini	*Saguinus midas*	2	2	0	0	MCZ	MS	40
Platyrrhini	*Saimiri sciureus*	3	1	1	1	MCZ	MS	47
Cercopithecidae	*Cercocebus torquatus*	2	2	0	0	AMNH	MS	90–120
Cercopithecidae	*Cercocebus galeritus*	1	1	0	0	AMNH, MCZ	MS	70
Cercopithecidae	*Cercopithecus mitis*	3	0	3	0	MCZ	MS	80
Cercopithecidae	*Chlorocebus pygerythrus*	3	1	2	0	SIU	MS	46–54
Cercopithecidae	*Colobus guereza*	3	1	2	0	AMNH	MS	66–73
Cercopithecidae	*Erythrocebus patas*	3	2	1	0	MCZ	MS	80
Cercopithecidae	*Lophocebus albigena*	3	1	2	0	MCZ	MS	90
Cercopithecidae	*Macaca fascicularis*	5	2	3	0	MCZ	MS	60–91
Cercopithecidae	*Mandrillus sphinx*	3	2	1	0	AMNH, MCZ	MS	75–126
Cercopithecidae	*Miopithecus talapoin*	3	3	0	0	MCZ	MS	50
Cercopithecidae	*Nasalis larvatus*	3	0	3	0	MCZ	MS	71

Cercopithecidae	*Papio anubis*	3	3	0	0	MCZ	MS	108–118
Cercopithecidae	*Piliocolobus badius*	3	2	1	0	MCZ	MS	80–90
Cercopithecidae	*Presbytis rubicunda*	3	1	2	0	MCZ	MS	80
Cercopithecidae	*Procolobus verus*	2	1	1	0	AMNH	MS	76–80
Cercopithecidae	*Semnopithecus entellus*	3	2	1	0	AMNH	MS	52–108
Cercopithecidae	*Simias concolor*	2	1	1	0	AMNH	MS	56
Cercopithecidae	*Theropithecus gelada*	3	2	1	0	AMNH	MS	84–120
Cercopithecidae	*Trachypithecus cristatus*	3	0	3	0	MCZ	MS	50
Hominidae	*Gorilla gorilla*	6	1	5	0	AMNH, MCZ	MS	106–131
Hominidae	*Pan paniscus*	5	1	3	1	AMNH, ICP, MCZ	MS, own data	66–116
Hominidae	*Pan troglodytes*	6	3	3	0	AMNH, ICP, MCZ	MS, own data	77–111
Hominidae	*Pongo* sp.	6	0	6	0	ICP, MCZ	MS, own data	77–125
Hylobatidae	*Hoolock hoolock*	3	1	2	0	AMNH	MS	52–84
Hylobatidae	*Hylobates agilis*	1	0	0	1	ICP	MS, own data	52
Hylobatidae	*Hylobates lar*	4	0	4	0	MCZ	MS	67
Hylobatidae	*Nomascus leucogenys*	1	1	0	0	AMNH	MS	105
Hylobatidae	*Symphalangus syndactylus*	2	0	2	0	AMNH	MS	62–79

Abbreviations: M = male; F = female; ? = unknown sex; AMNH = American Museum of Natural History, New York, USA; DUEA = Duke University, Evolutionary Anthropology, Durham, USA; ICP = acronym of the collections of the Institut Català de Paleontologia Miquel Crusafont, Sabadell, Spain; MCZ = Museum of Comparative Zoology, Harvard University, Cambridge, USA; MS = MorphoSource (https://www.morphosource.org); SIU = Southern Illinois University, Carbondale, USA; USNM = Smithsonian National Museum of Natural History, Washington, D.C., USA.

Table 2

Definition of the petrosal/tympanic landmarks used in this paper for aligning the specimens.

No.	Landmark	Definition
1	Porion	Most superior point on the margin of the external auditory meatus
2	Inferior external auditory meatus	Most inferior point on the margin of the external auditory meatus
3	Posterior external auditory meatus	Most posterior point on the margin of the external auditory meatus
4	Posterior internal auditory meatus	Most posterior point on the margin of the internal auditory meatus
5	Anterior internal auditory meatus	Most anterior point on the margin of the internal auditory meatus
6	Medial anterior pyramidal ridge	Most medial point where anterior pyramidal ridge starts running laterally above the fossa for the semilunar ganglion
7	Intersection ridge-groove	Point of intersection between the laterally running anterior pyramidal ridge and the groove of the greater petrosal nerve
8	Greater petrosal nerve hiatus	Most superior, anterior point on the margin of the hiatus for the greater petrosal nerve
9	Stylomastoid foramen	Center of the stylomastoid foramen

Table 3

Descriptive statistics of the variables describing the orientation, proportions and course of the carotid canal in the main extant anthropoid clades. See SOM Table S2 for the individual values of extant anthropoid specimens.

Clade	*n*	2DYZA			2DXYA			$L/V^{(1/3)}$			bgPC1			bgPC2		
		Mean	SD	Range	Mean	SD	Range	Mean	SD	Range	Mean	SD	Range	Mean	SD	Range
Platyrrhini	39	64.06	7.33	50.66–79.36	31.92	7.57	8.25–44.26	3.68	0.39	2.90–4.42	-0.36	0.11	0.50–0.07	-0.01	0.11	-0.26–0.17
Cercopithecidae	54	69.71	7.42	57.2–85	16.69	10	-3.54–33.87	2.86	0.42	1.40–3.87	0.17	0.08	-0.11–0.34	-0.04	0.09	-0.29–0.14
Hominidae	23	54.90	7.83	37.27–69.11	13.74	7.38	-0.82–27.78	3.23	0.31	2.57–3.82	0.12	0.08	-0.10–0.20	0.12	0.05	-0.01–0.20
Hylobatidae	11	54.51	12.39	38.27–78.27	10.27	7.44	1.00–23.27	2.68	0.47	1.97–3.37	0.18	0.08	0.06–0.32	-0.04	0.10	-0.25–0.12

Abbreviations: 2DYZA = 2D angle in the YZ plane (canal superior orientation; in degrees); 2DXYA = 2D angle in the XY plane (canal medial orientation; in degrees); L = length (in mm); V = volume (in mm^3); bgPC = between-group principal component.

Table 4

Variables describing the orientation, proportions and course of the carotid canal in the fossil specimens.

Species	Catalog No.	2DYZA	2DXYA	$L/V^{(1/3)}$	bgPC1	bgPC2
Ekembo heseloni	KNM-RU 2036al	53.58	34.73	3.12	-0.02	-0.03
Epipliopithecus vindobonensis	NHMW 1970/1397/0003	53.59	27.62	3.05	-0.08	-0.06
Pliobates cataloniae	IPS58443.1	35.58	16.86	3.58	-0.03	0.05
Victoriapithecus macinessi	KNM-MB 29100	66.73	10.36	3.25	-0.02	-0.04

Abbreviations: 2DYZA = 2D angle in the YZ plane (canal superior orientation; in degrees); 2DXYA = 2D angle in the XY plane (canal medial orientation; in degrees); L = length (in mm); V = volume (in mm^3); bgPC = between-group principal component.

Table 5

Z-score analysis of the three variables describing the orientation, proportions and course of the carotid canal in the fossil specimens and compared to the variation expressed by the main extant anthropoid clades.[a]

Variable and species	Catalog No.	Platyrrhini	Cercopithecidae	Hominidae	Hylobatidae
2DYZA					
Ekembo heseloni	KNM-RU 2036al	-1.43	**-2.17**	-0.17	-0.08
Epipliopithecus vindobonensis	NHMW 1970/1397/0003	-1.43	**-2.17**	-0.17	-0.07
Pliobates cataloniae	IPS58443.1	**-3.88**	**-4.60**	**-2.46**	-1.52
Victoriapithecus macinnesi	KNM-MB 29100	0.36	-0.40	1.51	0.98
2DXYA					
Ekembo heseloni	KNM-RU 2036al	0.37	1.80	**2.84**	**3.29**
Epipliopithecus vindobonensis	NHMW 1970/1397/0003	-0.56	1.09	1.88	**2.33**
Pliobates cataloniae	IPS58443.1	**-1.99**	0.02	0.42	0.89
Victoriapithecus macinnesi	KNM-MB 29100	**-2.85**	-0.63	-0.46	-0.02
$L/V^{(1/3)}$					
Ekembo heseloni	KNM-RU 2036al	-1.46	0.61	-0.36	0.93
Epipliopithecus vindobonensis	NHMW 1970/1397/0003	-1.64	0.44	-0.58	0.78
Pliobates cataloniae	IPS58443.1	-0.27	1.69	1.09	1.89
Victoriapithecus macinnesi	KNM-MB 29100	-1.13	0.91	0.04	1.20
bgPC1					
Ekembo heseloni	KNM-RU 2036al	**3.23**	**-2.30**	-1.78	**-2.39**
Epipliopithecus vindobonensis	NHMW 1970/1397/0003	**2.70**	**-2.97**	**-2.50**	**-3.08**
Pliobates cataloniae	IPS58443.1	**3.14**	**-2.41**	-1.90	**-2.51**
Victoriapithecus macinnesi	KNM-MB 29100	**3.19**	**-2.35**	-1.83	**-2.45**
bgPC2					
Ekembo heseloni	KNM-RU 2036al	-0.25	0.02	**-3.16**	0.04
Epipliopithecus vindobonensis	NHMW 1970/1397/0003	-0.51	-0.31	**-3.78**	-0.27
Pliobates cataloniae	IPS58443.1	0.48	0.93	-1.47	0.87
Victoriapithecus macinnesi	KNM-MB 29100	-0.25	0.02	**-3.17**	0.03

Abbreviations: 2DYZA = 2D angle in the YZ plane (canal superior orientation; in degrees); 2DXYA = 2D angle in the XY plane (canal medial orientation; in degrees); L = length (in mm); V = volume (in mm^3); bgPC = between-group principal component.

[a] Significant z-scores at $p < 0.05$ are bolded.

Table 6

Phylogenetic generalized least-squares (PGLS) allometric regressions between carotid canal size variables (L, $V^{1/3}$ or CS) or between carotid canal size and BM, together with PGLS bivariate regressions between carotid canal shape (as represented by the canal robusticity index or bgPCs) vs. log-transformed carotid canal size or BM.

Regression	p[a]	R^2	Slope	Slope 95% CI
ln L vs. ln $V^{1/3}$	<0.001	0.81	0.86	0.73, 0.99
ln L vs. ln $V^{1/3}$ [b]	<0.001	0.81	0.95	0.81, 1.10
$L/V^{1/3}$ vs. ln CS	>0.05	-0.02	0.11	–0.34, 0.57
ln L vs. ln CS	<0.001	0.99	1.04	1.02, 1.06
ln $V^{1/3}$ vs. ln CS	<0.001	0.81	0.99	0.84, 1.13
ln L vs. ln BM	<0.001	0.68	0.25	0.20, 0.31
ln $V^{1/3}$ vs. ln BM	<0.001	0.90	0.30	0.27, 0.34
ln CS vs. ln BM	<0.001	0.69	0.25	0.19, 0.30
$L/V^{1/3}$ vs. ln BM	<0.01	0.14	-0.17	–0.29, –0.05
bgPC1 vs. ln CS	>0.05	0.01	0.12	–0.07, 0.31
bgPC1 vs. ln $V^{1/3}$	<0.01	0.19	0.26	0.10, 0.41
bgPC1 vs. ln BM	<0.001	0.25	0.10	0.05, 0.15
bgPC2 vs. ln CS	<0.001	0.58	0.21	0.16, 0.27
bgPC2 vs. ln $V^{1/3}$	<0.001	0.46	0.17	0.11, 0.23
bgPC2 vs. ln BM	<0.001	0.35	0.05	0.04, 0.08

Abbreviations: L = carotid canal length (mm); $V^{1/3}$ = carotid canal volume cube root (mm); $L/V^{1/3}$ = shape index of canal robusticity; CS = carotid canal centroid size (mm); BM = body mass (g); bgPC = between-group principal component (representing carotid canal course).

[a] Regressions are significant when $p < 0.05$.

[b] For ln L vs. ln $V^{1/3}$, a major axis regression was also computed to test whether the two variables are isometric when deviation from the best-fit line is minimized simultaneously for both variables (instead of only the dependent variable, in this case ln L). Our results show that, unlike for the PGLS regression (which displays slight negative allometry), isometry cannot be discounted for the major axis regression.

Table 7

Number (*n*) and percentages (%) of correctly and incorrectly classified individuals obtained by the between-group principal components analysis after cross-validation. In total, 98 out of 127 (77.2%) individuals were correctly classified (in bold).

	Platyrrhini	Cercopithecidae	Hominidae	Hylobatidae
Platyrrhini	**36 (92.3%)**	0 (0%)	0 (0%)	3 (7.7%)
Cercopithecidae	1 (1.9%)	**34 (63.0%)**	9 (16.7%)	10 (18.5%)
Hominidae	0 (0%)	2 (8.7%)	**21 (91.3%)**	0 (0.0%)
Hylobatidae	0 (0%)	3 (27.3%)	1 (9.1%)	**7 (63.6%)**

Table 8

Posterior probabilities of group membership based on the between-group principal component scores of fossil specimens.[a]

Species	Catalog No.	Platyrrhini	Cercopithecidae	Hominidae	Hylobatidae
Ekembo heseloni	KNM-RU 2036al	<0.001	**0.098**	0.059	0.087
Epipliopithecus vindobonensis	NHMW 1970/1397/0003	<0.001	**0.018**	0.009	0.016
Pliobates cataloniae	IPS58443.1	<0.001	0.064	**0.169**	0.056
Victoriapithecus macinessi	KNM-MB 29100	<0.001	**0.089**	0.054	0.079

[a] Each value corresponds to the probability of having the given score if the specimen was a member of the group considered, not the likelihood of group membership in each of the a priori defined groups given a particular score (the greater the number, the higher the probability). For each specimen the highest probability is bolded.